Peptide Secondary Structure Folding Reaction Coordinate: Correlation between UV Raman Amide III Frequency, Ψ Ramachandran Angle, and Hydrogen Bonding

Aleksandr V. Mikhonin, Sergei V. Bykov, Nataliya S. Myshakina, and Sanford A. Asher*

Department of Chemistry, University of Pittsburgh, Pittsburgh, Pennsylvania 15260

Received: August 15, 2005; In Final Form: November 10, 2005

We used UV resonance Raman (UVRR) spectroscopy to quantitatively correlate the peptide bond $AmIII_3$ frequency to its Ψ Ramachandran angle and to the number and types of amide hydrogen bonds at different temperatures. This information allows us to develop a family of relationships to directly estimate the Ψ Ramachandran angle from measured UVRR $AmIII_3$ frequencies for peptide bonds (PBs) with known hydrogen bonding (HB). These relationships ignore the more modest Φ Ramachandran angle dependence and allow determination of the Ψ angle with a standard error of ±8°, if the HB state of a PB is known. This is normally the case if a known secondary structure motif is studied. Further, if the HB state of a PB in water is unknown, the extreme alterations in such a state could additionally bias the Ψ angle by ±6°. The resulting ability to measure Ψ spectroscopically will enable new incisive protein conformational studies, especially in the field of protein folding. This is because any attempt to understand reaction mechanisms requires elucidation of the relevant reaction coordinate(s). The Ψ angle is precisely the reaction coordinate that determines secondary structure changes. As shown elsewhere (Mikhonin et al. *J. Am. Chem. Soc.* **2005**, *127*, 7712), this correlation can be used to determine portions of the energy landscape along the Ψ reaction coordinate.

Introduction

The various techniques of molecular spectroscopy constitute the toolset used by scientists for investigating molecular conformations and reaction mechanisms. These various spectroscopic techniques require quantitative correlations between the spectral parameters measured and the molecular conformational parameters. NMR and especially multidimensional NMR techniques are certainly the most powerful spectroscopic methods for solution studies.[1−13] The origin of the power of NMR derives from its ultrahigh spectral resolutions and because the important spin interactions can be accurately modeled in terms of distances between atoms. The NMR techniques are certainly the gold standard methods for studying systems at high concentrations where the dynamical questions probed are slower than the microsecond time scale.[14,15]

In contrast, optical spectroscopic methods are used for lower concentration samples and for systems controlled by faster dynamics. For example, vibrational spectroscopic techniques can often be easily applied to studying low concentrations of species,[16−21] as well as to probe both very fast (femtosecond) and very slow processes.[22−34] Unfortunately, the resulting vibrational spectroscopic information cannot as easily be interpreted to obtain quantitative information on molecular conformation.[35] Although it is possible to calculate normal modes of large molecules in a vacuum, the uncertainties in these calculated frequencies and their assignments in the condensed phase prevent interpreting these results in terms of the molecular geometry present in the condensed phase. In general, the vibrational spectra are interpreted through indirect empirical arguments. It is unusual to be able to interpret vibrational spectra quantitatively by correlating measured vibrational spectral parameters to bond lengths, angles, etc.[36,37]

In the work here we have determined the frequency dependence of the Amide III (AmIII) band observed in the ∼200 nm UV resonance Raman (UVRR) spectra of peptides and proteins on the Ψ Ramachandran angle, which largely defines the peptide bond secondary structure.[22,38,39] The understanding of the dependence of the AmIII band on the Ψ Ramachandran angle has a long and distinguished history; almost 30 years ago Lord proposed that the AmIII band correlates with the peptide secondary structure.[40] During the succeeding years, numerous investigators have used this band to determine protein and peptide secondary structure.[38,39,41−58]

Recently Asher et al.[47] theoretically examined the dependence of the AmIII band on the Ψ angle and discovered that this dependence resulted from coupling between the peptide bond N−H and C_α−H in-plane bends. They found that this coupling varied sinusoidally with Ψ angle. They also discovered that there was much less dependence of the AmIII band on the Φ Ramachandran angle.[47,59] They also carefully examined[42] the amide III region of peptides and proteins and assigned a number of the bands in this region. They assigned one band in this spectral region, the $AmIII_3$ band, to the vibration whose frequency varies with the Ψ angle.[43,60] Further, they also recently showed that this Raman band derives from independent contributions from individual peptide bonds in the peptide and protein; there is no evidence of coupling of this vibration between adjacent peptide bonds,[61,62] unlike the commonly used AmI band.[61,63]

These observations are important because they indicate that the $AmIII_3$ band may be uniquely useful in peptide and protein conformational studies. This band is easily observed because it is strongly enhanced by resonance excitation in the peptide bond ∼200 nm $\pi \rightarrow \pi^*$ transitions.[39,64−66] Further, we showed that this band can be selectively measured for a single peptide bond by isotope editing the peptide or protein by replacing the C_α−H

* To whom correspondence may be sent. Phone: 412-624-8570. Fax: 412-624-0588. E-mail: asher@pitt.edu.

10.1021/jp054593h CCC: $33.50
Published on Web 01/10/2006

by $C_\alpha-D$.[42,47,67,68] The high S/N difference spectrum directly displays the $AmIII_3$ frequency.

In the work here we carefully examined the dependence of this $AmIII_3$ frequency on hydrogen bonding (HB), to separate the HB dependence from the Ψ angle dependence. This allows us to propose a family of relationships which can be used to determine the Ψ angle directly from the measured $AmIII_3$ frequency with a typical accuracy of $\pm 8°$, assuming a known HB state (however, see discussion below).

We are optimistic that these relationships will be very useful for protein conformational studies, especially in the field of protein folding. This is because any attempt to understand reaction mechanisms, such as, for example, protein folding, requires elucidation of the relevant reaction coordinate(s). The Ψ angle is precisely the reaction coordinate that determines secondary structure changes. As shown elsewhere[60] the correlation we propose can be used to experimentally determine features of the energy landscape along this Ψ reaction coordinate. Such an experimental insight into a protein conformation and energy landscape is crucially needed, since there are still a lot of unresolved questions regarding the theoretical modeling of protein folding despite remarkable recent achievments.[69−71]

Experimental Section

Sample Preparation. *N*-Methylacetamide (NMA, >99% pure) was purchased from Sigma Chemicals (St. Louis, MO) and used as received without any further purification. Neat liquid NMA (~13 M) and 0.13 M NMA in water solutions were used.

As described elsewhere,[43] the 21-residue alanine-based peptide $AAAAA(AAARA)_3A$ (AP) was prepared (HPLC pure) at the Pittsburgh Peptide Facility by using the solid-state peptide synthesis method. The AP solutions in water contained 1 mg/mL concentrations of AP, and 0.2 M concentrations of sodium perchlorate, which was used as an internal intensity and frequency standard.[22,29] All Raman spectra were normalized to the intensity of the ClO_4^- Raman band (932 cm^{-1}).

The undecapeptide XAO (MW = 985) was prepared (HPLC pure) at the Pittsburgh Peptide Facility by using the solid-state peptide synthesis method. The sequence of this peptide is Ac-XXAAAAAAAOO-amide, where all amino acids are in their L form, A is alanine, X is diaminobutyric acid (side chain CH_2-$CH_2NH_3^+$), and O is ornithine (side chain $(CH_2)_3NH_3^+$). We used 1 mg/mL solutions of XAO-peptide containing 0.15 M of sodium perchlorate. The UVRR spectra of XAO were also normalized to the ClO_4^- Raman band intensity.

As described elsewhere,[60] poly-L-lysine HCl (PLL, MW_{vis} = 28 500, MW_{LALLS} = 20 200) and the sodium salt of poly-L-glutamic acid (PGA, MW_{vis} = 17 000, MW_{mALLS} = 8853) were purchased from Sigma Chemical and used as received. Solution spectra of PLL and PGA were measured at pH = 2 and pH = 9, respectively, to ensure the absence of α-helix contributions. The mixed PLL and PGA neutral pH sample solutions contained identical concentrations of lysine and glutamic acid residues. These samples were freshly prepared before the Raman measurements. The total peptide concentrations were kept below 0.3 mg/mL to avoid gel formation.

UV Resonance Raman Instrumentation. The Raman instrumentation has been described in detail elsewhere.[22,72] A Coherent Infinity Nd:YAG laser produced 355 nm (third harmonic) 3 ns pulses at 100 Hz. This beam was Raman shifted to 204 nm (fifth anti-Stokes) by using a 1 m tube filled with hydrogen (60 psi). A Pellin Broca prism was used to select the 204 nm excitation beam. The Raman scattered light was imaged into a subtractive double spectrometer,[72] and the UV light was detected by a Princeton Instruments solar blind ICCD camera or a Roper Scientific UV CCD camera. All samples were measured in a thermostated free surface flow stream.

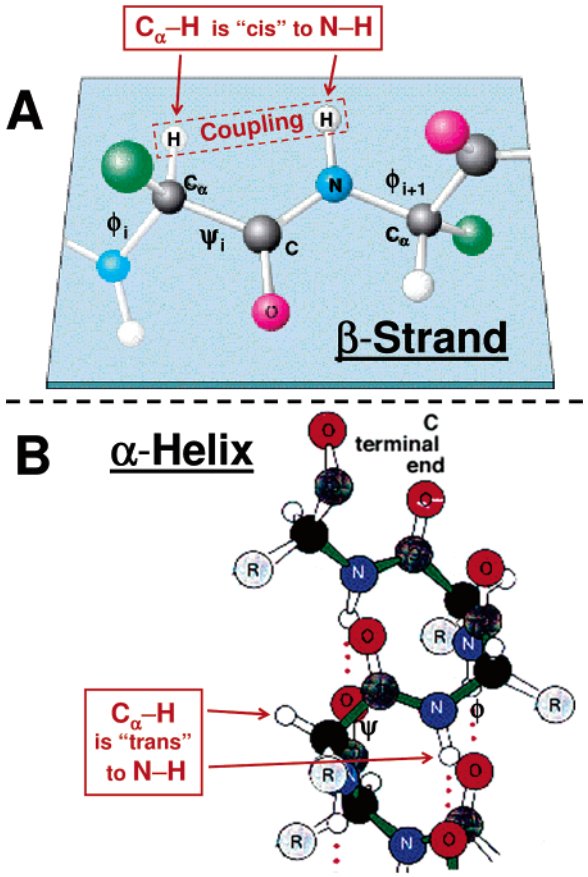

Figure 1. Model of a polypeptide chain (A) at β-strand-like and (B) at α-helix-like Ψ and Φ Ramachandran angles. The distance between $C_\alpha-H$ and N−H hydrogens depends on the Ψ Ramachandran angle.

Results and Discussion

Dependence of $AmIII_3$ Frequency on Ramachandran Angles and Hydrogen Bonding. The amide III (AmIII) band region is complex. We recently examined this spectral region in detail and identified a band, which we call $AmIII_3$ and which is most sensitive to the peptide bond conformation.[42] As briefly discussed in the Introduction, the peptide bond (PB) $AmIII_3$ frequency depends on its secondary structure which is defined by its Ψ and Φ Ramachandran angles.[43,47,59,73] The $AmIII_3$ frequency also depends on whether the PB hydrogen bonds (HBs) to water (HB_{P-W}),[74−77] or to other PBs (HB_{P-P}).[77−81] Although there is a modest Φ angle $AmIII_3$ frequency dependence, our studies to date show that the Ψ dependence dominates.[43,47,59] We discuss the relative Ψ and Φ angular dependencies in detail below. In addition, PB HBs to water leads to a characteristic temperature dependence[22,29,42,43] that derives from anharmonicities[25,82−87] in the PB and water HB potential functions (see Appendix for detail). Thus, we write

$$\nu_{III3} = \nu_{III3}(\psi,\phi,HB_{P-P},HB_{P-W},T) \quad (1)$$

$AmIII_3$ Frequency Dependence on Coupling between $C_\alpha-H$ and N−H Bending Motions. We showed earlier that the conformational sensitivity of the $AmIII_3$ band derives from coupling between the N−H and $C_\alpha-H$ bending motions.[47] For example, for β-strand-like Ψ and Φ Ramachandran angles the N−H and $C_\alpha-H$ bonds are approximately cis (Figure 1), which

gives rise to strong N−H to C_α−H bend coupling. In contrast, for α-helix-like Ψ and Φ Ramachandran angles the N−H and C_α−H bonds are approximately trans (Figure 1), and the N−H to C_α−H coupling disappears. The stronger the coupling, the lower the $AmIII_3$ frequency, as explained in detail elsewhere.[47]

This coupling between the N−H and C_α−H bending motions can be completely removed by C_α−D isotopic substitution because of the dramatically lowered C_α−D bending frequency. Ala-ala (AA) in water exists in a PPII-like conformation with Ψ and Φ angles of 132° and −67°, respectively.[88] The N−H and C_α−H bending motions strongly couple. C_α−D isotopic substitution in AA[47] results in a 68 cm^{-1} upshift of the $AmIII_3$ band frequency from 1270 to 1338 cm^{-1}. This occurs because of the loss of this strong coupling between the N−H and C_α−H bending motions. This shift upon C_α deuteration is also observed in the 21-residue mainly ala peptide (AP). Natural abundance AP in its unfolded state (essentially PPII, Ψ ≈ 145°, Φ ≈ −75°) shows the $AmIII_3$ band at 1252 cm^{-1} (at 0 °C).[42,43] 2,3,3,3-D_4 isotopic substitution (C_α−D, CD_3) results in a ∼74 cm^{-1} upshift of the $AmIII_3$ band to ∼1326 cm^{-1}.[42]

The extreme lowest frequency experimental value observed to date for the $AmIII_3$ frequency of 1227 cm^{-1} occurs in antiparallel β-sheet PB in water (Ψ ≈ 135°, Φ ≈ −139°) formed by PLL and PGA mixtures. Thus, it appears that the $AmIII_3$ frequency can be shifted by a maximum of ∼100 cm^{-1} due to this coupling of C_α−H and N−H bending motions.

The physical origin of this Ψ angle $AmIII_3$ frequency dependence is that the hydrogen van der Waals radii in the C_α−H and N−H bonds are in contact for positive Ψ angles (Figure 1), and the distance between the two H atoms shows a sinusoidal angular dependence. The coupling of these bending motions increases with the proximity of the hydrogen atoms. The coupling of bending motion causes a splitting of the vibrations into a high- and low-frequency component, the $AmIII_3$ band, and an anomalously enhanced C_α−H bending band which contains additional motions such as CO−N stretching.

Relative Impact of the Ψ and Φ Ramachandran Angles on the $AmIII_3$ Frequency. Although the projections of the N−H and C_α−H bending motions on each other (and as a result the degree of coupling between them) depend on *both* the Ψ and Φ Ramachandran angles, an examination of a model of a peptide bond (Figure 1) clearly shows that for the allowed regions of the Ramachandran plot only the Ψ angle directly alters the distance between the two hydrogens, while the Φ angle has little direct impact. Thus, for steric reasons alone we expect little influence on the $AmIII_3$ frequency due to variations in the Φ angle.

Asher et al.[47] theoretically investigated the Ψ angular dependence of $AmIII_3$ frequency in isolated alanine methylamide (AMA). AMA geometry was optimized at fixed Ψ angles using Gaussian 98W, and then the vibrational frequencies were calculated. This approach revealed the strong dependence of the AmIII frequency on the Ψ Ramachandran angle with a ∼61 cm^{-1} total span of calculated AmIII frequencies (∼74 cm^{-1} span from sinusoidal fit of these calculated data points, Figure 2).

Mirkin and Krimm[73] theoretically examined the Ψ and Φ frequency dependence of the AmIII band of "alanine dipeptide" (*N*-acetyl-L-alanine-*N*-methylamide). They concentrated on peptide bond 2, whose frequencies were close to those measured experimentally. Although Mirkin and Krimm claim in their conclusions, that AmIII frequency shows strong dependence on both Ψ and Φ Ramachandran angles, we note that the impact of changes in the Φ angle is relatively modest if we only include the allowed regions of the Ramachandran plot (Figure 3).

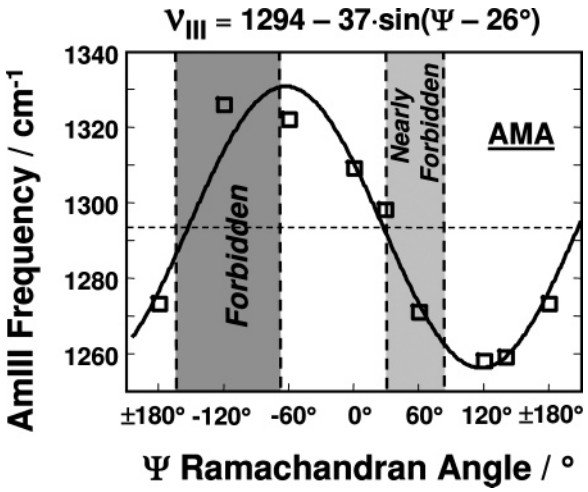

Figure 2. Black boxes (□): AmIII frequencies for isolated alanine methylamide (AMA) at fixed Ψ angles but with all the other parameters optimized, calculated by Gaussian 98W (see Asher et al.[47] for details). Black line (—): Fit of calculated points using the eq 3 (see text for detail). Note: Grey regions show the forbidden and/or nearly forbidden Ψ Ramachandran angles based on recent Ramachandran plots.[90−92]

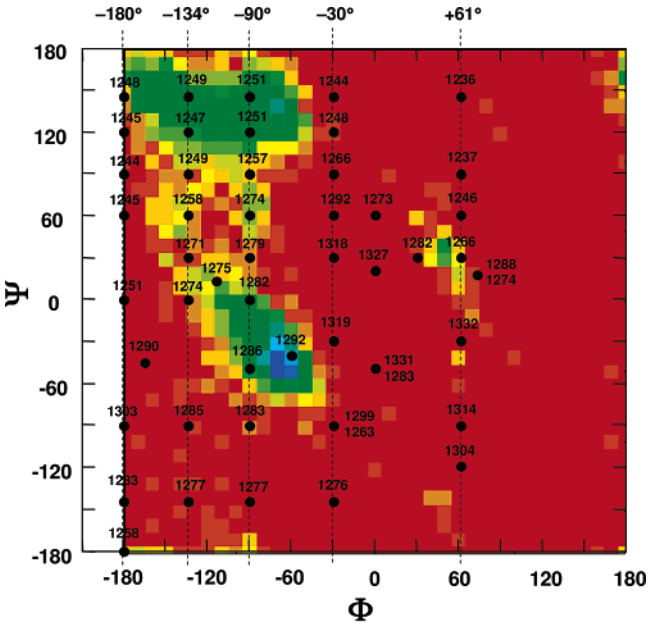

Figure 3. This AmIII vibrational frequency map for peptide group 2 of the alanine dipeptide is adapted from a figure by Mirkin and Krimm.[73] This map is overlaid with the recent Ramachandran plot for ala (obtained from http://alpha2.bmc.uu.se/gerard/rama/ramarev.html). The results show that over the allowed regions of Ramachandran plot the AmIII band shows a 3-fold greater frequency dependence on the Ψ angle than on the Φ angle.

In the allowed regions of Ramachandran plot, Mirkin and Krimm[73] calculated a 25−40 cm^{-1} AmIII frequency span over the allowed Ψ angles for fixed Φ angles (Figures 3 and 4). This 25−40 cm^{-1} Ψ angular frequency variation is somewhat lower than the 61 cm^{-1} span we[47] estimated for AMA. However, it is ∼3-fold greater than the 6−16 cm^{-1} AmIII frequency dependence calculated for the Φ angular dependence for fixed Ψ angles over the allowed regions of the Ramachandran plot (Figures 3 and 4).

In addition, the largest 16 cm^{-1} span in the AmIII frequency with Φ angle occurs in an almost forbidden region of the Ramachandran plot between the β-sheet and α-helical regions (at Φ angles of −134° and −90° and Ψ angle of 60°, Figures

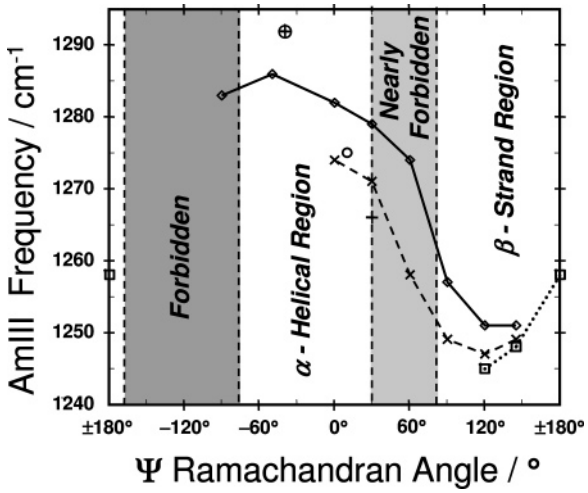

Figure 4. Ψ angular dependence of Mirkin and Krimm's[73] alanine−dipeptide AmIII frequencies at fixed Φ angles in the allowed regions of recent Ramachandran plot for ala (Figure 3, obtained from http://alpha2.bmc.uu.se/gerard/rama/ramarev.html): (□) at Φ = ±180°; (×) at Φ = −134°; (○) at Φ = −115°; (◇) at Φ = −90°; (plus sign in circle) at Φ = −60°; (+) at Φ = +61°. Note: Gray regions show the forbidden and/or nearly forbidden Ψ Ramachandran angles.

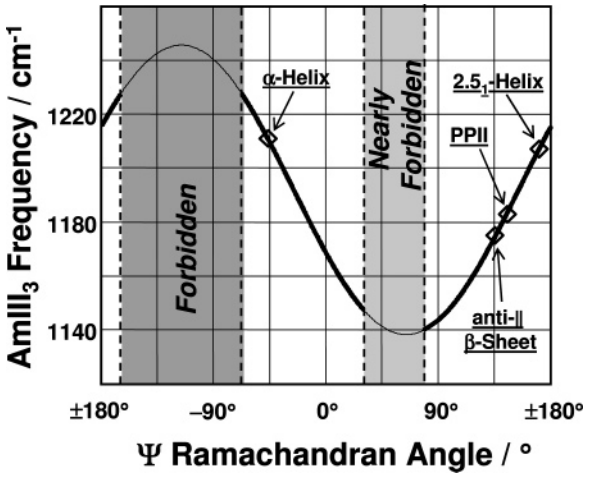

Figure 5. Refinement of correlation between $AmIII_3$ frequency and Ψ Ramachandran angle for non-HB PB, which reflects only coupling between N−H and C_α−H bending motions, as predicted earlier for AMA.[47] (A) (◇ $AmIII_3$ frequencies where the HB-induced frequency upshifts were subtracted from the experimentally measured values (see Appendix). (B) Black curve shows the best fit of these data (eq 5). Note: Gray regions show the sterically forbidden/nearly forbidden Ψ Ramachandran angles based on recent Ramachandran plots for non-Gly, non-Pro, and nonpre-Pro residues.[90−92]

3 and 4). In contrast, in the α-helical region of the Ramachandran plot the AmIII frequency of alanine dipeptide shows no more than 8 cm^{-1} Φ angular span, while in the *β*-strand region of the Ramachandran plot the AmIII frequency shows no more than 6 cm^{-1} Φ dependence (Figure 3).

Figure 4, which shows Mirkin and Krimm's[73] Ψ angular dependence of peptide bond 2 alanine dipeptide AmIII frequency at fixed Φ angles, emphasizes the dominance of the Ψ angular dependence in the allowed regions of the Ramachandran plot (Figure 3). Figure 4 indicates that in most of the *β*-strand region of the Ramachandran plot (Ψ = 120−180°) there is essentially a negligible dependence of the AmIII frequency on the Φ angle.

Ianoul et al.'s[59] combined experimental and theoretical studies of Ac−X−OCH_3 (X = Val, Ile, Leu, Lys, Ala) revealed a 9 cm^{-1} $AmIII_3$ frequency shift upon an 18° increase of the Φ Ramachandran angle from −96 to −78°. In addition, Ianoul et al. also performed theoretical calculations for Ala-Ala at a fixed α-helix-like Ψ angle of −21° and calculated only a 3 cm^{-1} $AmIII_3$ frequency upshift upon the 20° increase of Φ angle from −95° to −75°. Thus, Ianoul et al. never observed more than a 9 cm^{-1} shift of $AmIII_3$ frequency due to variation of the Φ Ramachandran angle.

In addition, we recently[60] measured the UVRR $AmIII_3$ frequencies of two different secondary structure conformations in aqueous solutions with very similar Φ angles, but very different Ψ angles. Specifically, an equimolar mixture of PLL and PGA forms an antiparallel *β*-sheet[60] (Ψ ≈ 135°, Φ ≈ −139°), which shows an $AmIII_3$ frequency at 1227 cm^{-1}. In contrast individual PLL and PGA samples form extended 2.5_1-helices[60] (Ψ ≈ 170°, Φ ≈ −130°), which show $AmIII_3$ frequencies at ∼1271 cm^{-1}. Figures 3 and 4 demonstrate that the entire frequency shift derives from changes in the Ψ Ramachandran angle alone; the 35° increase in the Ψ angle is mainly responsible for the large 44 cm^{-1} $AmIII_3$ frequency upshift. As discussed in detail in the Appendix, the difference in peptide HB in this case also has a minor impact on the $AmIII_3$ frequency difference.

To summarize, the total Φ angular span of the $AmIII_3$ frequencies appears experimentally[59] to be no more than 9 cm^{-1} and no more than 16 cm^{-1} in the allowed regions of the Ramachandran plot from theoretical calculations.[73] In contrast, Ψ angular span was observed to be as high as 44 cm^{-1} from the experiment (see above) and as high as 61 cm^{-1} from theoretical calculations[47] over the allowed region of the Ramachandran plot (Figure 2). We will show below that the Ψ Ramachandran angular span of the $AmIII_3$ frequency can be as high as 80 cm^{-1} in the allowed regions of the Ramachandran plot (Figure 5).

Thus, we conclude that Ψ **Ramachandran angular dependence of the $AmIII_3$ frequency dominates the Φ angular dependence in the allowed regions of Ramachandran plot.**

If we totally neglect the Φ angular dependence of $AmIII_3$ frequency, this could enable an error in the Ψ-dependent $AmIII_3$ frequency of no more than ±8 cm^{-1} (since the total Φ angular span of $AmIII_3$ frequencies no higher than 16 cm^{-1}, Figure 3). Thus, we can rewrite eq 1

$$\nu_{III3}(\psi,\phi,HB_{P-P},HB_{P-W},T) \cong \nu_{III3}(\psi,HB_{P-P},HB_{P-W},T) \quad (2)$$

It was already mentioned that the $AmIII_3$ frequency dependence on the Ψ Ramachandran angle results from the Ψ angular dependence of coupling between the N−H and C_α−H bending motions.[47] Our theoretical calculations of alanine methylamide (AMA) in a vacuum[47] showed that the extent of this coupling depends on the projections of these motions onto one another and that this dependence results in a sinusoidal-like $AmIII_3$ frequency dependence for a non-HB PBs

$$\nu_{III3}(\psi) \cong \nu_0 - A\sin(\psi - \alpha_0) \quad (3)$$

Further, we assume that the $AmIII_3$ frequency dependencies on its Ψ Ramachandran angle and on its HB are independent. Thus, we can rewrite eq 2

$$\nu_{III3}(\psi,HB_{P-P},HB_{P-W},T) \cong \{\nu_0 - A\sin(\psi - \alpha_0)\} + \Delta\nu_{III3}(HB_{P-P},HB_{P-W},T) \quad (4)$$

where $\Delta\nu_{III3}(HB_{P-P},HB_{P-W},T)$ is the $AmIII_3$ frequency shift due to the HB of the PB N−H and/or C═O groups.

Formation of PB−*water* and PB−PB HBs upshift the $AmIII_3$ frequency, in part, due to the resulting increased C(O)═N double

TABLE 1: Dependence of $AmIII_3$ Frequencies on Hydrogen Bonding (HB) for Different Secondary Structures at 20 °C (unless stated otherwise) under Conditions Specified

	$AmIII_3$ frequency (cm^{-1})			
	without any PB−PB and PB−*water* HB (in a vacuum)	with PB−PB HB, but without PB−*water* HB	in water, but without any PB−PB HB	both in water and with PB−PB HB
PPII ($\Psi = 145°$, $\Phi = -75°$)	1183	N/A	1247[a]	N/A
2.5_1-helix ($\Psi = 170°$, $\Phi = -130°$)	1207	N/A	1271[a]	N/A
α-helix internal residues ($\Psi = -47°$, $\Phi = -57°$)	1211	1258[a]	N/A	1263[a]
α-helix three terminal residues on C-terminus site ($\Psi = -47°$, $\Phi = -57°$)	1211	1246	N/A	1266
α-helix three terminal residues on N-terminus site ($\Psi = -47°$, $\Phi = -57°$)	1211	1223	N/A	1272
anti-∥ β-sheet all residues, which are two end-on PB−PB H-bonded (see text) ($\Psi = 135°$, $\Phi = -139°$)	1175	1222	N/A	1227[a]
anti-∥ β-sheet residues from exterior strands ($\Psi = 135°$, $\Phi = -139°$)	1175 1175	1210 1184	N/A N/A	1230 1236

[a] Measured Experimentally. The Appendix describes these frequency assignments in detail.

TABLE 2: $AmIII_3$ Frequency Upshifts for Different Peptide Secondary Structures Due to PB−*Water* and PB−PB HB at 0 °C with Respect to Non-HB PB in Vacuum

	$AmIII_3$ frequency upshift due to PB−*water* HB at specific sites,[a] cm^{-1}					$AmIII_3$ frequency upshift due to PB−PB HB at specific sites,[a] cm^{-1}			total $AmIII_3$ frequency upshift due to HB, cm^{-1}
secondary structure	$\Delta\nu^A$	$\Delta\nu^B$	$\Delta\nu^C$	$\Delta\nu^{D,D*}$	total	$\Delta\nu^E$	$\Delta\nu^F$	total	
PPII	15	33	16	N/A	64	N/A	N/A	N/A	64
2.5_1-helix	15	33	16	N/A	64	N/A	N/A	N/A	64
extended β-strand	15	33	16	N/A	64	N/A	N/A	N/A	64
AP solid state α-helix (dehydrated)	N/A	N/A	N/A	N/A	N/A	35	12	47	47
AP α-helix in water	N/A	N/A	N/A	5	5	35	12	47	52
PLL-PGA mixture anti-∥ β-sheet	N/A	N/A	N/A	5	5	35	12	47	52

[a] See Figures 10 and 15−17 as well as Appendix for detail.

bond character.[75,76] The magnitude of this $AmIII_3$ frequency upshift depends on whether C═O and/or N−H sites HB and whether these HB occur to water or to other PB. The Appendix below details our determinations of the $AmIII_3$ frequency shifts due to HB for all the common PB conformations and HB patterns. These considerations allow us to write three families of eqs 5, 6A−D, and 7A−C which display the dependence of the $AmIII_3$ frequency on the Ψ angle, on the PB HB and on temperature. **These relationships and Figures 5−7 can be used to determine the Ψ angle of a particular PB from its experimentally determined $AmIII_3$ frequency, given its known HB state with an error as discussed below.** In addition, we also developed the "average" eq 6E, if the HB state of a PB in water is unknown.

Determining these correlations between the $AmIII_3$ frequency and PB HB requires detailed considerations of the many HB states (see Appendix). To make the results of our study easily accessible to the reader, we first discuss the conclusions. We leave the discussion of the detailed considerations of the different HB patterns to a lengthy Appendix, which must be examined in order to judge the reliability of our conclusions.

The relationships given below by eqs 5 (for non-HB PB in a vacuum), 6A−D (PB in aqueous solutions), and 7A−C (PB in the absence of water) are shown in Figures 5, 6, and 7, respectively.

Correlation between $AmIII_3$ Frequency and Ψ Ramachandran Angle in the Absence of HB. We measured the UVR $AmIII_3$ frequencies for the AP α-helix[42,89] (∼1263 cm^{-1}, 0 °C), XAO PPII[42,43] (1247 cm^{-1}, 0 °C), PLL and PGA 2.5_1-helix[60] (∼1271 cm^{-1}, 0 °C), and PLL−PGA mixture antiparallel β-sheet[60] (∼1227 cm^{-1}, 0 °C) conformations of different polypeptides in aqueous solutions. Each of these conformations has known Ramachandran angles (Table 1).

We can calculate the $AmIII_3$ frequencies that would result from the above peptide conformations in the fictitious case where the PB did not partake in any HB at all. This would be done by subtracting the HB-induced $AmIII_3$ frequency shifts (Table 2), determined in the Appendix, from the experimentally measured $AmIII_3$ frequencies in aqueous solutions (Table 1). The resulting $AmIII_3$ frequencies for non-HB PB at corresponding Ψ Ramachandran angles are shown in the second column of Table 1. Removal of this HB dependence then allows us to refine our theoretically calculated frequency dependence of the $AmIII_3$ band on the Ψ angle dependent coupling between N−H and C_α−H bends (eq 3).

By fitting the above four "non-HB" data points to eq 3, we obtain the following semiempirical relationship, which relates

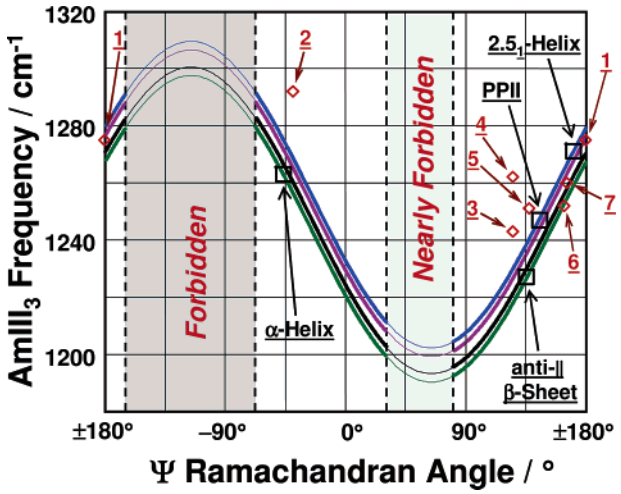

Figure 6. Correlation between $AmIII_3$ frequency, HB pattern, and Ψ Ramachandran angle: (□) measured $AmIII_3$ frequencies of α-helix, antiparallel β-sheet, PPII, and 2.5_1 helix in aqueous solutions; (◇) measured $AmIII_3$ frequencies of peptide crystals, plotted against their Ψ Ramachandran angles 1-Ala-Asp, 2-Gly-Ala-Leu·$3H_2O$, 3-Val-Glu, 4-Ala-Ser, 5-Val-Lys, 6-Ser-Ala, 7-Ala-Ala. Blue curve is a theoretically predicted correlation (eq 6A) for PB, which are fully exposed and fully HB to water (PPII, 2.5_1-helix, extended β-strand). Green curve is a theoretically predicted correlation (eq 6B) for PB, for two end-on PB−PB HB (infinite α-helix, interior strands of β-sheet). Magenta curve is a theoretically predicted correlation (eq 6C) for PB where only the C═O group has a PB−PB HB (example: three α-helix N-terminal PB, half of PB of the exterior strands of a β-sheet. Black curve is a theoretically predicted correlation (eq 6D) for PB with just their N−H group PB−PB HB (example: three α-helix C-terminal PB, the other half of PB of exterior strands of β-sheet).

the $AmIII_3$ frequency to the Ψ Ramachandran angle dependent coupling between N−H and C_α−H bending motions

$$\nu_{III3}(\psi) = [1192\ cm^{-1} - 54\ cm^{-1}\sin(\psi + 26°)] \quad (5)$$

Figure 5 shows the dependence of the $AmIII_3$ frequency on the Ψ angle as predicted by eq 5. The gray regions in Figure 5 (as well as in Figures 6 and 7) show the sterically forbidden Ψ Ramachandran angles based on revised Ramachandran map for non-Gly, non-Pro, and non-pre-Pro residues.[90−92]

Correlation of $AmIII_3$ Frequency and Ψ Ramachandran Angle for PB Fully Exposed to Water: PPII, 2.5_1-Helix, and Extended β-Strand. PB fully exposed to water, such as in the PPII, 2.5_1-helix and extended β-strand-like conformations, will HB to three waters/water clusters at sites A, B, C (Appendix, Figure 10). As discussed in the Appendix, this results in an $AmIII_3$ frequency upshift of 64 cm^{-1} (at $T = 0$ °C) compared to that predicted by eq 5. In addition, the $AmIII_3$ frequency will show a temperature dependence for these conformations[42,43,60] because the strength of the PB−*water* HB decreases as the temperature increases (see eqs 18−22 of the Appendix). Thus, we can write

$$\nu_{III3}^{EXT}(\psi,T,HB) = [1256\ cm^{-1} - 54\ cm^{-1}\sin(\psi + 26°)] - 0.11\frac{cm^{-1}}{°C}(T - T_0)\} \quad (6A)$$

where $T_0 = 0$ °C

The blue curve in Figure 6 shows the dependence of the $AmIII_3$ frequency on Ψ angle as predicted by eq 6A at $T = 0$ °C for these water-exposed conformations. The experimentally observed $AmIII_3$ frequencies of the XAO PPII (0 °C) and PLL or PGA 2.5_1-helix (0 °C) lie on this curve.

Correlation of $AmIII_3$ Frequency and Ψ Ramachandran Angle for Two-End-On PB−PB HBs: Infinite α-Helix, Interior Strands of β-Sheet in Water. Each PB in infinitely long α-helices and in interior strands of multistranded β-sheets in aqueous solutions (Appendix, Figures 14 and 15) will partake in two-end-on PB−PB HBs at sites E and F. In the Appendix we show that in this case the $AmIII_3$ frequency upshifts by 47 cm^{-1} for α-helix and β-sheet due to PB−PB HBs (Table 2, Figure 15). It upshifts an additional 5 cm^{-1} in both α-helices and β-sheets due to an additional PB−water HB producing a total HB-induced upshift of 52 cm^{-1} (Table 2, Figure 15). In addition, there is essentially no temperature dependence for the $AmIII_3$ frequency for the long α-helix[42,89] and multistranded β-sheet[60] conformations (see Appendix, eq 25). Thus, we include a 52 cm^{-1} HB-induced shift to eq 5 and write

$$\nu_{III3}^{i\alpha,i\beta}(\psi,T_0,HB) = [1244\ cm^{-1} - 54\ cm^{-1}\sin(\psi + 26°)] \quad (6B)$$

The green curve in Figure 6 shows the predicted eq 6B behavior. The experimentally observed $AmIII_3$ frequencies of the AP α-helix and the PLL−PGA antiparallel β-sheet conformations (dominated by interior strands) lie on this curve.

Correlation of $AmIII_3$ Frequency and Ψ Ramachandran Angle for PB Where Only the C═O Group Participates in PB−PB HBs: Three N-Terminal α-Helix PB, Half of PB of Exterior Strands of β-Sheet in Water. The three N-terminal PBs of α- helices and half of the PBs of exterior strands of β-sheets (Appendix, Figures 14 and 16) will have just their C═O groups HB to PB (with possibly an additional C═O HB to water). In contrast, their N−H groups will HB to water clusters. In the Appendix (Figure 16) we estimate that the $AmIII_3$ upshift is 61 cm^{-1} (with respect to the same PB, which does not partake in any HB). As discussed in the Appendix we expect a smaller temperature dependence (see discussion below eq 26 in Appendix) than for the fully water HB PB. Thus, we can write

$$\nu_{III3}^{e\alpha1,e\beta1}(\psi,T,HB) = [1253\ cm^{-1} - 54\ cm^{-1}\sin(\psi + 26°)] - 0.08\frac{cm^{-1}}{°C}(T - T_0) \quad (6C)$$

The magenta curve in Figure 6 shows the behavior of eq 6C at $T = 0$ °C. We do not, at present, have any experimentally measured data points for peptides with the HB patterns considered in eq 6C. However, experimentally measured UVRR spectra of double-stranded β-sheet and/or short α-helices must contain contributions from such HB conformations.

Correlation of $AmIII_3$ Frequency and Ψ Ramachandran Angle for PB in Which Only the N−H Group Participates in PB−PB HBs: Three C-Terminal α-Helix PBs, Other Half of PB of Exterior Strands of β-Sheet in Water. The three C-terminal PBs of α-helices and the other half of the PBs of the exterior strands of β-sheet (Appendix, Figures 14 and 17) will have just their N−H groups HB to another PB at site E, while their C═O groups will be HB to water at sites A and C. In the Appendix we estimate that in this case the HB-induced $AmIII_3$ upshift is 55 cm^{-1} (Figure 17). In addition, we estimate the temperature dependence to be half that of the PPII conformation (discussion below eq 26). Thus, we can add 55

TABLE 3: UVRR AmIII$_3$ Frequencies and X-ray Ψ and Φ Ramachandran Angles for Peptide Crystals

	AmIII$_3$ frequency, cm^{-1}	Ψ Ramachandran angle, deg	Φ Ramachandran angle, deg
Gly-Ala-Leu·3H$_2$O	1292	−40	−67
Ala-Ser (anhydrous)	1262	125	−157
Val-Glu (anhydrous)	1243	125	−82
Val-Lys (anhydrous)	1251	137	−105
Ser-Ala (anhydrous)	1252	163	−80
Ala-Ala (anhydrous)	1260	165	−113
Ala-Asp (anhydrous)	1275	179	−113

cm^{-1} HB-induced upshift as well as the temperature-dependent term to eq 5 and write

$$\nu_{III3}^{e\alpha 2,e\beta 2}(\psi,T,\mathrm{HB}) = [1247\ \mathrm{cm}^{-1} - 54\ \mathrm{cm}^{-1}\sin(\psi + 26°)] - 0.05\frac{\mathrm{cm}^{-1}}{°\mathrm{C}}(T - T_0) \quad (6D)$$

The black curve in Figure 6 shows the behavior of eq 6D. We do not, at present, have any experimentally measured data points for peptides with the HB patterns considered in eq 6D. However, experimentally measured UVRR spectra of double-stranded β-sheet and/or short α-helices will contain contributions from these HB conformations.

Correlation of AmIII$_3$ Frequency and Ψ Angle for a PB in Water If Its HB State Is Unknown. If the HB state of a PB in aqueous solution is unknown, we suggest the use of eq 6E, which is the "average" of eqs 6A−D. This will minimize the error in determination of the Ψ Ramachandran angle and will allow the estimation of the Ψ angle with the error bounds discussed below.

$$\nu_{III3}^{EXT}(\psi,T,\mathrm{HB}) = [1250\ \mathrm{cm}^{-1} - 54\ \mathrm{cm}^{-1}\sin(\psi + 26°)] - 0.06\frac{\mathrm{cm}^{-1}}{°\mathrm{C}}(T - T_0)\} \quad (6E)$$

Correlation between AmIII$_3$ Frequency and Ψ Ramachandran Angle in Peptide Crystals. Figures 6 and 7 show the correlation of the previously measured[42] AmIII$_3$ frequencies and the Ramachandran Ψ angles for crystal powders of the three anhydrous dipeptides Val-Lys, Ala-Ala, and Ala-Asp, and three new anhydrous dipeptides Ser-Ala, Val-Glu, and Ala-Ser, as well as for a hydrated crystal[43] powder of Gly-Ala-Leu·3H$_2$O (GAL). The structures of these peptides are known from single-crystal X-ray diffraction measurements.[93−99] We grew the crystal powders and measured the lattice constants using powder pattern X-ray diffraction. If our lattice constants matched that of known crystal structures confirmed, we assumed the published crystal structure Ψ and Φ angles (Table 3).

Figures 6 and 7 show that the crystal data appear to roughly follow the sinusoidal relationship between the AmIII$_3$ frequency and the Ψ Ramachandran angle (see red dashed curve in Figure 7); however, the crystal data are systematically upshifted. This upshift is largest when comparing the data to the green, black, and magenta theoretical curves in Figure 7, where the curves model PB−PB HB in the absence of water. The systematic upshifts in the crystal frequencies almost certainly result from the different types, numbers, and increased strengths of HB in these peptide crystals. Specifically, in these di- and tripeptide crystals,[93−99] N−H groups of PB usually HB to carboxylates instead of carbonyls (as in longer peptides), while C═O groups of PB usually HB to N−H$_3^+$ groups instead of N−H groups (as in longer peptides). Despite sharing many common features,

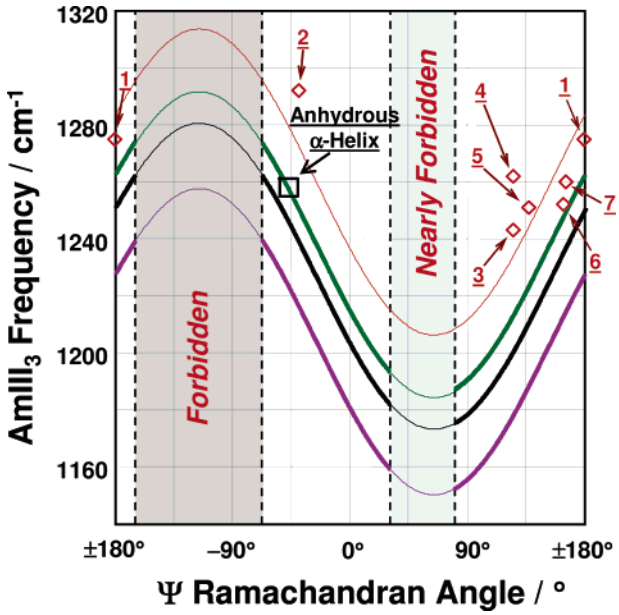

Figure 7. Correlation between AmIII$_3$ frequency, HB pattern, and Ψ Ramachandran angle for lyophilized anhydrous peptides: (□) measured AmIII$_3$ frequencies of anhydrous AP α-helix; (◇) measured AmIII$_3$ frequencies of peptide crystals, plotted against their Ψ Ramachandran angles 1-Ala-Asp, 2-Gly-Ala-Leu·3H$_2$O, 3-Val-Glu, 4-Ala-Ser, 5-Val-Lys, 6-Ser-Ala, 7-Ala-Ala. Green curve is theoretically predicted correlation (eq 7A) for anhydrous PB with two end-on PB−PB HB (infinite α-helix, interior strands of β-sheet). Magenta curve is theoretically predicted correlation (eq 7B) for anhydrous PB where only the C═O group has a PB−PB HB (example: three N-terminal PB of anhydrous α-helix, half of PB of the exterior strands of an anhydrous β-sheet). Black curve is theoretically predicted correlation (eq 7C) for anhydrous PB with just their N−H group PB−PB HB (example: three C-terminal PB of anhydrous α-helix, the other half of PB of exterior strands of anhydrous β-sheet).

the HB patterns of these peptide crystals differ from each other. Thus, some scatter of AmIII$_3$ frequencies in these crystals (Figures 6 and 7) probably occurs due to these differences in HB. We are presently attempting to understand these affects in detail, but for the moment we only use these data to further indicate the veracity of our correlations.

Anhydrous α-Helical and β-Sheet Conformations. If we dehydrate a two-end-on PB−PB HB α-helical conformation, we will see a 5 cm^{-1} AmIII$_3$ frequency downshift due to the loss of hydrogen bonding to the normally present sheath of water.[89] In this case we can subtract out 5 cm^{-1} from the eq 6B and write the eq 7A (see also Figure 15 of Appendix)

$$\nu_{III3}^{i\alpha,i\beta}(\psi,T_0,\mathrm{HB}) = [1239\ \mathrm{cm}^{-1} - 54\ \mathrm{cm}^{-1}\sin(\psi + 26°)] \quad (7A)$$

The Figure 7 green curve shows the eq 7A relationship. The square data point in Figure 7 indicates Pimenov et al.[89] AmIII$_3$ frequency of an anhydrous α-helix AP sample (Table 1) as discussed in detail in the Appendix (Figure 15).

In the case of a PB where only the C═O group is involved in PB−PB HB, we estimate that the AmIII$_3$ frequency is 12 cm^{-1} upshifted with respect to non-HB PB (Appendix, Figure 16). This would be the case for the three N-terminal PBs of anhydrous α-helices and for half of the PB of the exterior strands of anhydrous β-sheets (Appendix, Figures 14 and 16). Thus, we can write

$$\nu_{III3}^{e\alpha 1,e\beta 1}(\psi,T_0,\mathrm{HB}) = [1204\ \mathrm{cm}^{-1} - 54\ \mathrm{cm}^{-1}\sin(\psi + 26°)] \quad (7B)$$

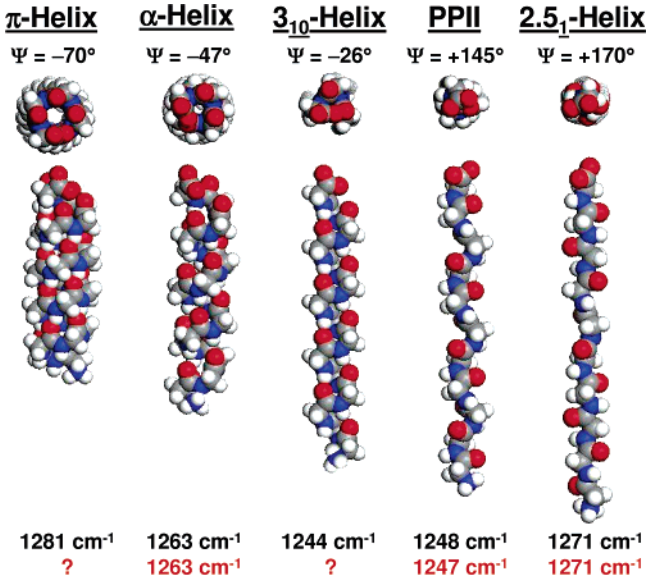

Figure 8. Predicted $AmIII_3$ frequencies (black numbers) from the Ψ Ramachandran angles and HB patterns for different types of helices in water. Red numbers: measured $AmIII_3$ frequencies at 0 °C. Equation 6B was used for PPII and 2.5_1 helices. Equation 6C was used for π-, α-, and 3_{10}-helices.

The Figure 7 magenta curve shows the eq 7B relationship.

In the case of PB, where only the NH group is PB−PB HB, we estimate the $AmIII_3$ frequency to be 35 cm^{-1} upshifted with respect to non-HB PB (Appendix, Figure 17). This would be the case for the three C-terminal PB of anhydrous α-helix and half of the PB of the exterior strands of the anhydrous β-sheet (Figures 14 and 17 of Appendix). Thus, we can write

$$\nu_{III3}^{e\alpha1,e\beta1}(\psi,T_0,\mathrm{HB}) = [1227\ \mathrm{cm}^{-1} - 54\ \mathrm{cm}^{-1}\sin(\psi + 26°)] \quad (7C)$$

The black curve in Figure 7 shows the eq 7C relationship.

The impact of different HB patterns, reflected by eqs 7A−C, produces much greater differences in $AmIII_3$ frequencies under anhydrous conditions compared to those in aqueous solutions (compare Figures 6 and 7), since PB−*water* HB-induced $AmIII_3$ frequency upshifts do not compensate for the differences in PB−PB HB-induced upshifts. It should be also noted that eqs 7A−C behavior will only dominate the behavior of relatively long, anhydrous, lyophilized peptides.

Thus, the families of eqs 6A−D and 7A−C predict the correlation between the $AmIII_3$ frequency and the Ψ angle for the common conformations of peptides and proteins. If the HB is known for a particular PB, the appropriate equation can be used to determine its Ψ angle from the observed $AmIII_3$ frequency. In the case where the HB state of a PB in aqueous solution is unknown, one can use eq 6E. These relationships will become less accurate if the PB has an unusual Φ angle or unusual HB pattern (see below).

Prediction of UVRR $AmIII_3$ Frequencies of Other Secondary Structures. On the basis of the known Ψ Ramachandran angle and HB patterns, we can predict the $AmIII_3$ frequencies of other secondary structures such as the π-helix, 3_{10}-helix (Figure 8), parallel β-sheet, and various turns (Figure 9). Using eq 6B, we predict ∼1281, ∼1244, and ∼1209 cm^{-1} $AmIII_3$ frequencies for two end-on PB−PB HB π-helix (Ψ = −70°), 3_{10}-helix (Ψ = −26°), and parallel β-sheet (Ψ = +113°) in water, respectively.

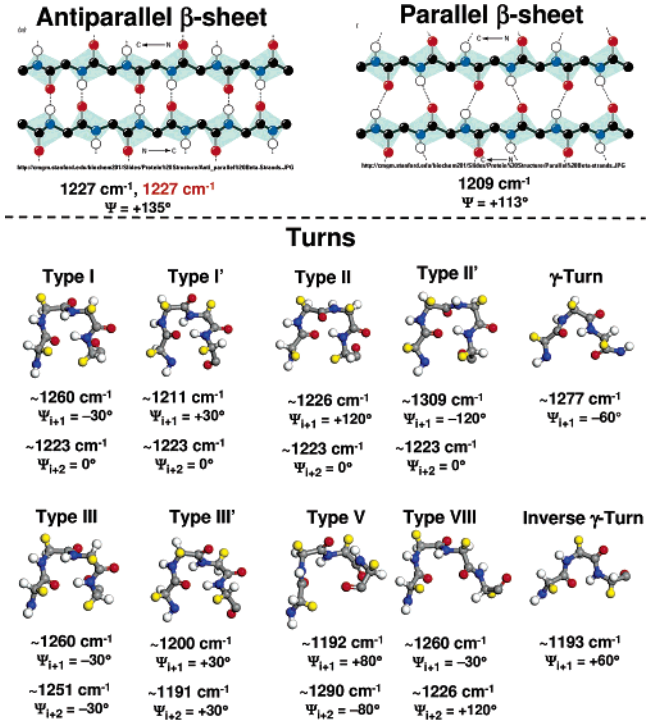

Figure 9. Predicted $AmIII_3$ frequencies from Ψ Ramachandran angle and HB pattern for interior strands of antiparallel and parallel β-sheets in water as well as that of different types of turns (black numbers). Measured $AmIII_3$ frequencies of PLL−PGA antiparallel β-sheet, dominated by interior strands (red number). Pictures of β-sheets were taken from http://cmgm.stanford.edu/biochem201/Slides/.

Figure 9 displays our estimates for interior strands of β-sheets and different turns in water. For the γ-turn we predict an $AmIII_3$ band at 1277 cm^{-1} (eq 6D), for an inverse γ-turn at 1193 cm^{-1} (eq 6D). Assuming that the different PBs in the chain contribute to UVRR spectra independently from their neighbors,[61,62] we predict the following: for a type I turn we predict $AmIII_3$ bands at 1260 (eq 6A) and 1223 cm^{-1} (eq 6D) for the $(i + 1)$ and $(i + 2)$ PBs in the turn, respectively; for a type I′ turn we predict 1211 (eq 6A) and 1223 cm^{-1} (eq 6D) for the two PBs in the turn, respectively; for a type II turn we predict 1226 (eq 6A) and 1223 cm^{-1} (eq 6D) for the two PBs in the turn; for a type II′ turn we predict 1309 (eq 6A) and 1223 cm^{-1} (eq 6D) for the two PBs in the turn; for a type III turn we predict 1260 (eq 6A) and 1251 cm^{-1} (eq 6D) for the two PBs in the turn; for a type III′ turn we predict 1200 (eq 6A) and 1191 cm^{-1} (eq 6D) for the two PBs in the turn; for a type V turn we predict 1192 (eq 6B) and 1290 cm^{-1} (eq 6D) for the two PBs in the turn; for a type VIII turn we predict 1260 (eq 6A) and 1226 cm^{-1} (eq 6A) for the two PBs in the turn.

UVRR spectra of HEWL amyloid fibrils,[100] which are dominated by β-sheet conformations contain three spectroscopic features in the $AmIII_3$ region: ∼1210, ∼1230, and ∼1255 cm^{-1}. The dominating ∼1230 cm^{-1} feature certainly derives from antiparallel β-sheet, though a minor contribution of several turn conformations is also possible (Figure 9). The ∼1255 cm^{-1} feature probably derives from turn conformations. Our results above suggest that a type I turn, or rare types III and VIII turns, could contribute to the ∼1255 cm^{-1} feature of HEWL (Figure 9). The ∼1210 cm^{-1} feature most likely derives from aromatic amino acid side chains, whose vibrations are enhanced with 197 nm excitation. However, there could be some contribution from either type I′ turn or type III′ turns (Figure 9).

Ψ Ramachandran Angle Determination Error Estimates. To estimate the likely error and bias in the determination of

the Ψ angle from the Raman measurements, we have to analyze the likely errors in the determination of the $AmIII_3$ frequency of the peptide bond of interest, as well as the error associated with the theoretical relationships that neglect the Φ dependence of the $AmIII_3$ frequency. In the simplest case, where we have only one amide bond, our error is determined by the error in resolving the $AmIII_3$ band from the $AmIII_2$ band and other adjacent interfering bands. In the case of homopeptides we often attempt to determine the band frequency from a particular conformation, which presents the increased complexity of resolving between the $AmIII_3$ bands of multiple conformations. Finally, we expect to be challenged by the case where we specifically examine the $AmIII_3$ band of a particular peptide bond in a polypeptide or protein. In this case, for example, we isotopically substitute the $C_\alpha-H$ of that peptide bond and compare the spectra of the natural abundance and the isotopic derivative to model the difference spectrum to selectively determine the peptide bond $AmIII_3$ frequency.

Thus, the likely error is very sample dependent and derives from the spectral S/N and the reliability of our modeling. In fitting, the resulting standard deviation of the fit depends on peak overlap and spectral S/N. Typically our spectral fitting, assuming Voigt profiles, calculates standard deviations of $\sim 2-3$ cm^{-1} in the majority of cases; it is never more than ~ 7 cm^{-1}, even in the most unfavorable cases. The derivative of the Ψ angle with respect to the $AmIII_3$ frequency: $\partial\Psi/\partial\nu \cong 1°/cm^{-1}$ over essentially all of the allowed values of Ψ (Figures 5−7). Thus, we obtain measurement error standard deviations in the determined Ψ angles of $\sim 2-3°$ for most cases and extreme standard deviations of $\sim 7°$ for rare unfavorable cases.

The error associated with neglecting the Φ angle also gives rise to the uncertainty in the Ψ angle determination. Ianoul et al.[59] theoretically and experimentally showed that different Φ angles could cause a maximum 9 cm^{-1} shift of the $AmIII_3$ frequency, while Mirkin and Krimm[73] indicates a potential span of AmIII frequency as much as 16 cm^{-1} in the allowed regions of Ramachandran plot (Figure 3). However, in the β-strand region of the Ramachandran plot we find that a Φ span is less than ~ 6 cm^{-1}, while that in the α-helix region is less than ~ 8 cm^{-1} (Figure 3). Thus, the extreme maximum spans of Ψ angle which could occur by neglecting the Φ angle is $\sim 16°$. Thus, the extreme standard error of Ψ angle associated with the neglecting the Φ angle is $\pm 8°$ (for an average Φ angle). Further, for the most abundant secondary structure motifs from the α-helical and β-strand regions of the Ramachandran plot, the Φ angle associated errors are only $\pm 4°$ and $\pm 3°$, respectively.

Additional bias can occur if we do not know the HB state of a PB in water. This could give rise to a bias of the $AmIII_3$ frequency of ± 6 cm^{-1}, which would lead to a Ψ angle bias of $\pm 6°$ in eq 6E. **Thus, a typical UV Raman measurement of a typical sample would find a random error of $\leq \pm 8°$ in the Ψ angle, assuming a known HB state.** However, extreme alterations in the unknown HB state of a PB in water could additionally bias the Ψ angle by $\pm 6°$.

Conclusions

We used UV resonance Raman spectroscopy to investigate the dependence of the $AmIII_3$ frequency on the Ψ Ramachandran angle and on the nature of PB HBs. These results allow us to formulate relationships that allow us to estimate the Ψ Ramachandran angles from observed $AmIII_3$ frequencies for both aqueous solutions of peptides and proteins as well as for the anhydrous states of peptides and proteins. **A typical Raman measurement of a typical sample would find a random error of $\leq \pm 8°$ in the Ψ angle, assuming a known HB state.** However, if the HB state of a PB in water is unknown, extreme alterations in such a state could additionally bias the Ψ angle by $\pm 6°$.

We are optimistic that these relationships will be very useful for protein conformational studies, especially in the field of protein folding. This is because any attempt to understand reaction mechanisms, such as protein folding, requires elucidation of the relevant reaction coordinate(s). The Ψ angle is precisely the reaction coordinate that determines secondary structure changes. As shown elsewhere,[60] the correlation we propose can be used to determine features of the energy landscape along this Ψ reaction coordinate.

Acknowledgment. We thank Dr. Igor Lednev, Dr. Simon Lovell, and Dr. Anatoli Ianoul for helpful discussions as well as NIH Grant 8 RO1 EB002053021 for financial support.

Appendix

In this Appendix we carefully investigate the dependence of $AmIII_3$ frequency on the Ψ Ramachandran angle, the peptide bond−water hydrogen bonding (PB−water HB), and the peptide bond−peptide bond hydrogen bonding (PB−PB HB) based on both experimental and theoretical studies. These considerations allow us to quantitatively characterize the HB-induced $AmIII_3$ frequency shifts (summarized in Table 2) in the cases of the common protein/peptide secondary structure conformations. Then, we subtract these HB-induced shifts from the experimentally measured UVRR $AmIII_3$ frequencies for pure secondary structure conformations (Table 1), to refine Asher et al.'s theoretically predicted[47] sinusoidal correlation between the $AmIII_3$ frequency and the Ψ Ramachandran angle (eq 3). The reason we neglect the Φ angular dependence of $AmIII_3$ frequency is explained in great detail above.

Dependence of $AmIII_3$ Frequency on PB HB. In *N*-methylacetamide (NMA), theoretical calculations[75,76] show that the formation of a single N−H PB−*water* HB upshifts the AmIII band by $\sim 17-20$ cm^{-1}, while formation of a C═O PB−*water* HB upshifts the AmIII frequency only $11-13$ cm^{-1}. Qualitatively, similar shifts should occur for PB−PB HB. However, N−H group PB−PB HB are somewhat stronger than PB−*water* N−H group HB.[101] In contrast, C═O group PB−PB HB have strengths similar to individual PB−*water* C═O HB.[101] To complicate things, the total AmIII frequency shift nonlinearly depends both on the number of PB HB formed and on their individual strengths.[75,76] For example, three simultaneous waters HB to a PB result in a larger AmIII frequency upshift than the sum of upshifts of the individual HBs.

Recently[42] we identified the $AmIII_3$ band in peptides and proteins, the normal mode composition of which is essentially similar to that of "classical" AmIII band of NMA. Figure 10, which shows the possible water HB geometries to a PB, indicates the estimated hydrogen bond $AmIII_3$ frequency shift for each possibility.

PB−*water* HB gives rise to a large temperature dependence of the $AmIII_3$ frequency[22,29,42,43] due to anharmonicities.[25,82−87] A significantly smaller temperature dependence of the $AmIII_3$ frequency occurs for α-helix and β-sheet peptides because they are extensively PB−PB HB.[22,42,43,60,89] This difference occurs between NMA dissolved in water and pure NMA, where the pure NMA HBs only to other NMA molecules (Table 4).

Figure 11 compares the 204 nm UVRR spectra of neat liquid NMA to a 0.13 M solution (1 vol %) of NMA in water at high and low temperatures. We find that the neat NMA AmII and

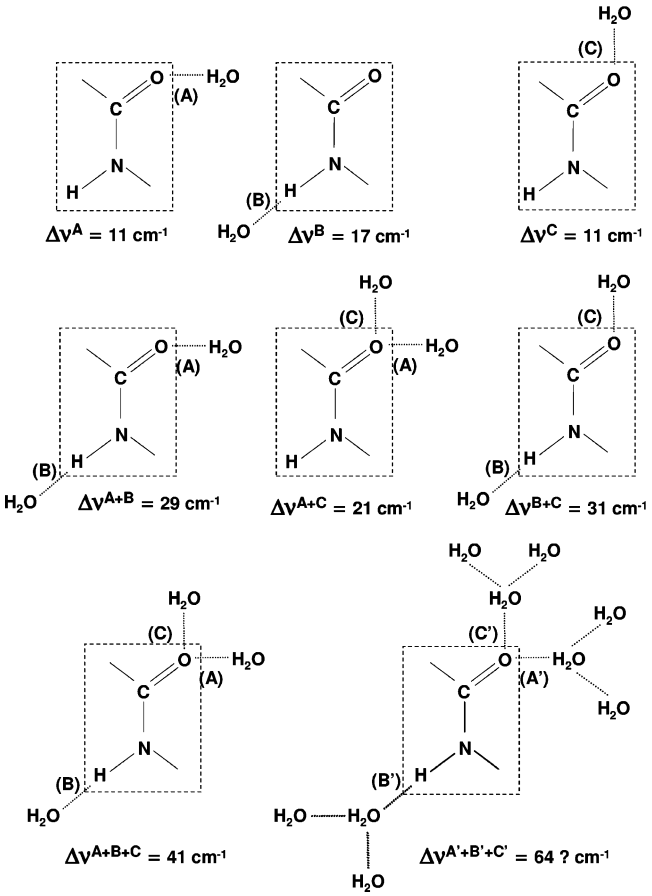

Figure 10. $AmIII_3$ upshifts due to PB−*water* HB in the case of fully exposed PB, i.e., for PPII, 2.5_1-helix, and extended β-strand conformations. Note that water can HB to the PB at sites A, B, and C. The values of these upshifts derive from calculations of NMA by Torii et al.[76] and measurements by Kubelka and Keiderling.[74] The largest shift of 62 cm^{-1} at room temperature (or 64 cm^{-1} for NMA in water at 0 °C, Table 4) is measured by Kubelka and Keiderling. These upshifts are explained in terms of water cluster hydrogen bonding by the very recent important paper of Schmidt et al.[77]

TABLE 4: Frequencies and Temperature Dependencies of 204 nm UVRR Amide Bands of Neat NMA and 0.13 M (1 vol %) NMA in Water

	NMA, neat liquid		0.13 M NMA in water	
amide band	ν at 79 °C, cm^{-1}	$\Delta\nu/\Delta T$, cm^{-1}/°C	ν at 70 °C, cm^{-1}	$\Delta\nu/\Delta T$, cm^{-1}/°C
AmIII	1293	-0.05 ± 0.01	1309	-0.09 ± 0.01
AmII	1558	-0.069 ± 0.015	1574	-0.11 ± 0.01
AmI	1668	$+0.04 \pm 0.01$	1649	$+0.01 \pm 0.03$[a]

[a] It is hard to accurately determine the temperature dependence of AmI band of 0.13 M NMA in water due to overlap between strong AmII and weak AmI bands (see Figure 11).

AmIII frequency shifts/°C are ∼40% less than that those of NMA in water (Table 4), showing that the impact on the $AmIII_3$ frequency of the anharmonicity in the PB−PB HB is less than that of PB−*water* HB.[42,43] PBs fully exposed to water usually have three PB−*water* HBs (Figure 12, I).[75−77,102] Two water molecules HB to the PB C═O group at sites A and C, while a third water molecule HBs to the PB N−H group at site B.[75,76] Monte Carlo simulation studies of NMA hydration[103] show that the NMA is dominantly HB to three waters at sites A, B, and C as shown in Figure 10.

PB−PB HB is dominated by two-end-on HBs[77,104−107] between the N−H and C═O groups at sites E and F (Figure 12, II). We recently showed that formation of an additional PB−*water* HB to the PB C═O groups at sites D and D* (Figure 12, II) gives rise to an additional ∼5 cm^{-1} frequency upshift.[89] This smaller ∼5 cm^{-1} upshift results from water HB simultaneously at sites D and D* because the D* water hydrogen bond weakens the C═O to H−N HB (Figure 9 of Schmidt et al.[77]).

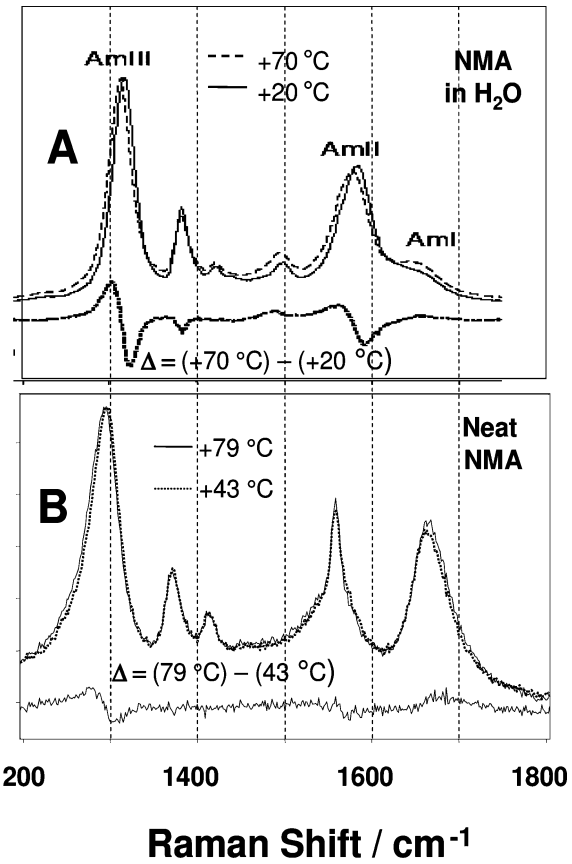

Figure 11. 204 nm UVRR spectra of NMA at high and low temperatures as well as their difference spectra (high (low T): (A) 0.13 M NMA in water at +20 and +70 °C; (B) NMA neat liquid at +43 and +79 °C. Sharp band at ∼1555 cm^{-1} originates from atmospheric O_2.

Thus, the resulting $AmIII_3$ HB-induced frequency dependence in eq 4 is

$$\Delta\nu(HB_{P-W},HB_{P-P},T) \cong \{n^{A}\,\Delta\nu^{A}_{P-W}(T) + n^{B}\,\Delta\nu^{B}_{P-W}(T) + n^{C}\,\Delta\nu^{C}_{P-W}(T)\} + \{n^{F}\,\Delta\nu^{F}_{P-P}(T) + n^{E}\,\Delta\nu^{E}_{P-P}(T) + n^{D,D^*}\,\Delta\nu_{P-W}{}^{D,D^*}(T)\} \quad (8)$$

where $\Delta\nu^{A,B,C,D,D^*}_{P-W}(T)$ are the temperature-dependent $AmIII_3$ frequency shifts due to HBs of individual water molecules to specific sites A, B, C or D and D* (Figures 10 and 12); $\Delta\nu^{E,F}_{P-P}(T)$ are the temperature-dependent $AmIII_3$ frequency shifts due to individual PB−PB HBs at NH and/or CO sites (Figure 12); n^{A,B,C,D,D^*} and $n^{E,F}$ are the coordination numbers, which are equal to "1" if a particular site HB and "0" otherwise.

In the work here we will concentrate on exploring the two cases where the PB either is fully exposed to water (PPII, 2.5_1-helix and extended β-strand conformations), or is involved in two-end-on PB−PB HBs, as in an infinite α-helix or multiple-stranded β-sheet conformation. We assume that the N−H HB is completely fulfilled by one HB of either type, while the C═O may have one or two HBs. If a PB is fully exposed to water, its N−H will always HB to one water/water cluster, while its C═O will always HB to two waters/water clusters (Figure

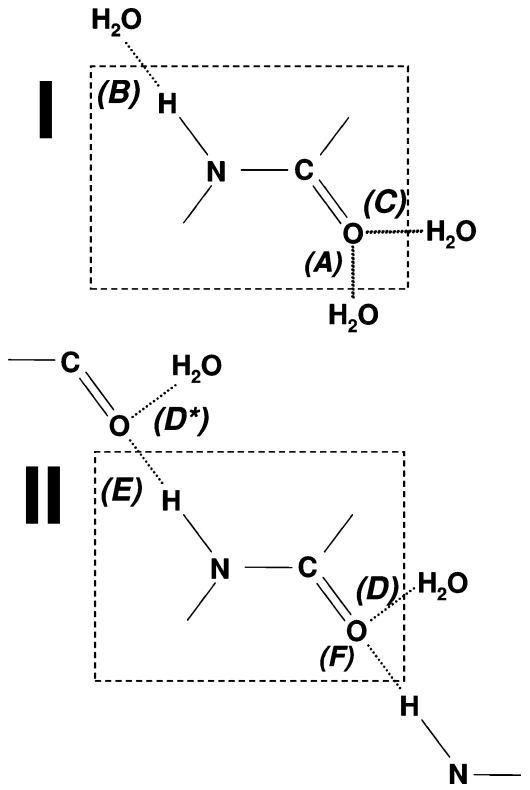

Figure 12. Definitions of all possible HB sites for (I**)** a PB, which is fully exposed to water (PPII, 2.5_1-helix and extended β-strand), and (II**)** a PB, with two PB−PB end-on HB (as in the interior PBs of an α-helix, and PBs of interior strands of β-sheet).

12, I). Thus, in *eq 8 if* $n^A = n^B = n^C = 1$*, then we define* $n^D = n^{D^*} = n^E = n^F = 0$.

If the PB N−H is HB to another PB, it cannot additionally HB (Figure 12, II). Thus, *in eq 8 if* $n^E = 1$*, then* $n^B = 0$ *and vice versa)*. If the C═O of a PB is HB to another PB, it cannot HB to an additional PB, but it can additionally HB to water at site D, depending upon its water exposure (Figure 12, II).

Thus, eq 4 can be rewritten inserting eq 8

$$\nu_{\mathrm{III3}}(\psi, \mathrm{HB_{P-P}}, \mathrm{HB_{P-W}}, T) \cong [\nu_{\mathrm{VAC}}(\psi{=}0) - A_c \sin(\psi - \alpha_C)] + [n^A \Delta\nu^A_{\mathrm{P-W}}(T) + n^B \Delta\nu^B_{\mathrm{P-W}}(T) + n^C \Delta\nu^C_{\mathrm{P-W}}(T)] + [n^E \Delta\nu^E_{\mathrm{P-P}}(T) + n^F \Delta\nu^F_{\mathrm{P-P}}(T) + n^{D,D^*} \Delta\nu^{D,D^*}_{\mathrm{P-W}}(T)] \quad (9)$$

where $\nu_{\mathrm{vac}}(\psi{=}0)$ is the $\mathrm{AmIII_3}$ frequency of a non-HB PB in a vacuum with $\psi = 0°$. A_c measures the impact on the $\mathrm{AmIII_3}$ frequency of the coupling between the N−H and C_α−H bending motions.

We found that maximum coupling occurs at a Ψ Ramachandran angle[43] of ∼+85°, where the C_α−H and N−H bonds are approximately cis, while a minimum coupling occurs for an α-helix-like Ramachandran angles[43,47] of Ψ ∼ −95° (in a sterically forbidden region of Ramachandran surface), where these bonds are essentially trans.

We now need to quantitatively characterize the remaining parameters of eq 9.

Dependence of $\mathrm{AmIII_3}$ Frequency on PB−Water HB (PPII, 2.5_1 Helix, and Extended β-Strand Conformations). Kubelka and Keiderling's[74] experimental studies of NMA hydration indicate that the AmIII frequency of fully hydrated NMA at room temperature is 62 $\mathrm{cm^{-1}}$ upshifted, compared to that of gas-phase NMA at ∼100 °C. Taking into account the slope of temperature-induced coefficients (Table 4), we estimate the AmIII frequency upshift from the high-temperature gas-phase NMA to 0 °C NMA in water to be 64 $\mathrm{cm^{-1}}$ (Figure 10). However, the theoretical studies of Besley[75] and Torii et al.[76] suggest somewhat lower upshifts of 54 and 41 $\mathrm{cm^{-1}}$ for NMA HB to the three individual water molecules at sites A, B, and C. We think that a larger experimental PB−*water* HB-induced shift of NMA occurs in real liquid water, since water clusters rather than the individual water molecules HB to NMA (especially at low temperatures), increasing the actual PB−*water* HB strength (Figure 10).

Calculations of Schmidt et al.[77] also suggest that HB of a three-water cluster to site B results in a 20 $\mathrm{cm^{-1}}$ larger upshift of the AmII band of NMA, than occurs upon HB of one water to site B. Table 4 shows, that temperature slope of the AmIII frequency shifts/°C of NMA (which are measures of the temperature dependence of the HB strength) are ∼25% less than that of AmII. Thus, we estimate an additional upshift for the AmIII band due to HB to the water cluster compared to that of one water at site B to be $\sim 0.75 \times 20 = 15$ $\mathrm{cm^{-1}}$. This is consistent with Kubelka and Keiderling's[74] FTIR measurements which suggest that the upshift of the NMA AmIII band (62 $\mathrm{cm^{-1}}$) from the gas phase to water solution is ∼75% of that of the NMA AmII band upshift (83 $\mathrm{cm^{-1}}$). Thus, HB of NMA to water clusters, instead of to individual water molecules at sites A, B, and C, additionally increases the AmIII frequency upshift from 41 to 62 $\mathrm{cm^{-1}}$ at room temperature or to ∼64 $\mathrm{cm^{-1}}$ at 0 °C (Figure 10).

The situation becomes more complex for PBs of long peptides and proteins, since different side chains and different secondary structural motifs will show different water exposures of C═O and N−H groups. Thus, we will need to carefully specify the HB pattern for each PB for these systems.

The PPII structure, which is an extended structure with all of its PBs fully exposed to water, appears to be mainly stabilized by PB−*water* interactions.[108−110] The PPII conformation has three waters/water clusters HB at each A, B, and C PB site, like that of NMA. Thus, we expect that the PPII conformation will show an $\mathrm{AmIII_3}$ HB-induced frequency shift from vacuum to water similar to that of NMA. Figure 10 shows our estimated $\mathrm{AmIII_3}$ frequency upshifts for all possible HB to water situations; we estimate that the $\mathrm{AmIII_3}$ frequency of fully hydrated PPII at $T_0 = 0$ °C will be ∼64 $\mathrm{cm^{-1}}$ upshifted relative to the PPII chain in a vacuum, similar to that of NMA.[74]

Thus, hydration of the PPII conformation gives rise to a shift of

$$\Delta\nu^{\mathrm{PPII}}_{\mathrm{P-W}}(A,B,C,T_0) = \Delta\nu^{\mathrm{MAX}}_{\mathrm{P-W}}(T_0) \approx \Delta\nu^{\mathrm{A}}_{\mathrm{P-W}}(T_0) + \Delta\nu^{\mathrm{B}}_{\mathrm{P-W}}(T_0) + \Delta\nu^{\mathrm{C}}_{\mathrm{P-W}}(T_0) \cong 64\ \mathrm{cm^{-1}} \quad (10)$$

We recently discovered 2.5_1-helix conformations of PLL and PGA, which are stabilized by charged side chain electrostatic repulsions.[60] These almost fully extended conformations have Ramachandran angles not far from those of the PPII conformation and show a similar water exposure (based on monotonic frequency shifts[60]) with three water/water clusters HB to the PB. Thus, we expect the 2.5_1-helix $\mathrm{AmIII_3}$ frequency will also be 64 $\mathrm{cm^{-1}}$ upshifted from vacuum to water (Tables 1 and 2)

$$\Delta\nu^{2.5_1}_{\mathrm{P-W}}(A,B,C,T_0) \approx \Delta\nu^{\mathrm{PPII}}_{\mathrm{P-W}}(T_0) \cong 64\ \mathrm{cm^{-1}} \quad (11)$$

We also expect a similar result for all water-exposed extended β-strand structures

$$\Delta\nu^{\mathrm{EXTENDED}}_{\mathrm{P-W}}(A,B,C,T_0) \approx \Delta\nu^{\mathrm{PPII}}_{\mathrm{P-W}}(T_0) \cong 64\ \mathrm{cm^{-1}} \quad (12)$$

Assuming that the PB of these extended β-strand-like structures HB to water clusters, rather than to single water molecules, we can quantitatively estimate the individual HB $AmIII_3$ upshifts at site A, B, and C from the AmII upshifts of Schmidt et al.[77] The HB-induced upshifts of $AmIII_3$ band are ~75% of the AmII frequency upshifts (see discussion above).

However, the sum of the $AmIII_3$ upshifts, estimated from the Shmidt et al.[77] AmII upshifts, is slightly lower than the empirically obtained 64 cm^{-1} upshift (eq 12). This is consistent with theoretical studies of Besley[75] and Torii et al.,[76] which propose that the three simultaneous PB−*water* HBs at sites A, B, and C result in a slightly higher $AmIII_3$ frequency upshift than the sum of upshifts due to the individual HBs. For simplicity, we neglect this nonlinearity and estimate the parameters in eq 10 as $\Delta\nu^{A}_{P-W} = 15\ cm^{-1}$, $\Delta\nu^{B}_{P-W} = 33\ cm^{-1}$, and $\Delta\nu^{C}_{P-W} = 16\ cm^{-1}$ to make their sum equal to 64 cm^{-1}. Thus, in the case of a fully exposed to water extended β-strand structure, we write

$$\Delta\nu_{III3}(T_0,\mathrm{HB}) = n^{A}_{P-W}\cdot 15\ cm^{-1} + n^{B}_{P-W}\cdot 33\ cm^{-1} + n^{C}_{P-W}\cdot 16\ cm^{-1} \quad (13)$$

where $T_0 = 0$ °C.

Dependence of $AmIII_3$ Frequency on Peptide Bond−Peptide Bond HB in Neat NMA. We can estimate the influence of PB−PB HBs on the $AmIII_3$ frequency directly from the experimentally measured AmIII frequencies of neat NMA and NMA in water (Figure 11, Table 4). NMA in water shows a 1315 cm^{-1} AmIII frequency at 0 °C, 64 cm^{-1} upshifted with respect to that in a vacuum[74] at 1251 cm^{-1}. There seems to be some systematic difference between the gas-phase NMA 1255 cm^{-1} value reported by Kubelka and Keiderling[74] and the 1259 cm^{-1} value reported by Mayne and Hudson.[111]

The NMA AmIII frequency upshifts from 1251 cm^{-1} in the gas phase to 1295 cm^{-1} in the neat liquid (at +40 °C) is caused by PB−PB HB. Neat NMA solutions are dominated by NMA clusters with only two PB−PB HBs.[104,106,107] Thus, utilizing the temperature-induced frequency shifts of Table 4, we estimate a 46 cm^{-1} $AmIII_3$ frequency upshift at 0 °C due to PB−PB HB

$$\Delta\nu^{NMA}_{P-P}(T_1) \approx \Delta\nu^{E}_{P-P}(T_1) + \Delta\nu^{F}_{P-P}(T_1) \cong 46\ cm^{-1} \quad (14)$$

since $n^{E} = n^{F} = 1$.

Alternatively, Schmidt et al.'s.[77] calculations predict a 43 cm^{-1} NMA AmII upshift upon N−H PB−PB HBs at site E and 16 cm^{-1} AmII upshift upon C═O PB−PB HBs at site F. Recalling[74] that $\Delta\nu_{III} \approx 0.75\Delta\nu_{II}$, we can estimate the AmIII frequency upshifts due to NH (site E) and C═O (site F) PB−PB HB as 35 + 12 cm^{-1}= 47 cm^{-1}, respectively. Our third independent estimate of the $AmIII_3$ upshift due to PB−PB HB in antiparallel β-sheet (see eq 16) gives the value of 48 cm^{-1}. These values are very close to the 46 cm^{-1} value measured for NMA (Figures 11 and 13). We will use the 47 cm^{-1} value for PB−PB HB-induced $AmIII_3$ frequency upshifts, since it is the average of these three estimates.

Despite the theoretical studies,[75,76] which propose that two simultaneous HBs to NH and C═O groups of a PB may result in a slightly higher $AmIII_3$ frequency upshift than the sum of upshifts due to the individual HB, we for simplicity estimate the NMA parameters in eq 13 as $\Delta\nu^{E}_{P-P} = 35\ cm^{-1}$, while $\Delta\nu^{F}_{P-P} = 12\ cm^{-1}$.

Dependence of $AmIII_3$ Frequency on α-Helix HB. The ideal α-helix conformation has the *i*th residue N−H group intramolecularly HB to the $(i + 4)$th residue C═O group (Figure 14). In addition, there is evidence of HB of the exposed PBs to the surrounding sheath of waters.[80,81,89,105,112−114] The three C-terminal α-helix residues have just their N−H groups intramolecularly HB (Figure 14), while the three N-terminal α-helix residues have just their C═O groups intramolecularly HB (Figure 14). Since each PB contributes to the AmIII Raman bands independently from their neighbors,[61] the UVRR spectra of an α-helix of seven or more residues long will have contributions from three differently HB PBs, which have the same α-helix Ramachandran angles (Figures 15−17).

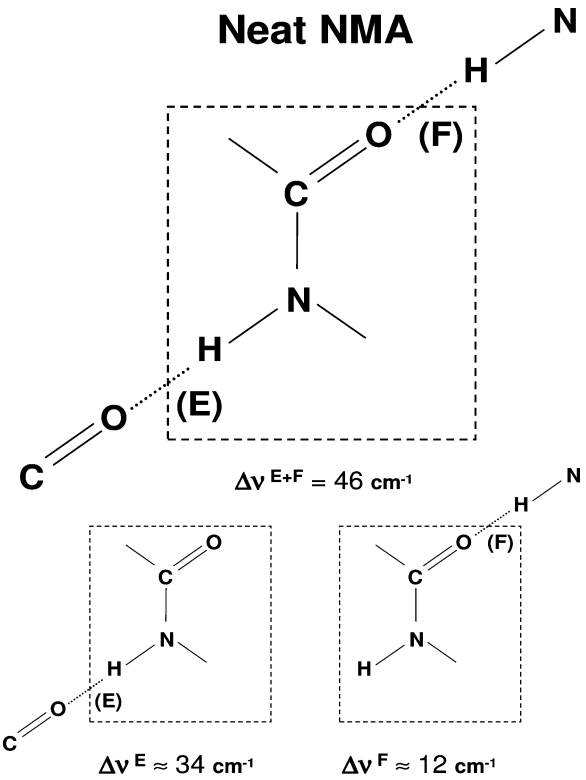

Figure 13. $AmIII_3$ frequency upshifts due to N−H (site E) and C═O (site F) PB−PB HB in neat NMA. Note: ~48 cm^{-1} AmIII upshift for two end-on PB−PB HB was measured, while the AmIII upshifts for PB−PB HB at individual sites E and F were estimated from their AmII band upshifts.[77]

We expect the $AmIII_3$ frequency of the PB of interior residues, which have two-end-on PB−PB HBs at their C═O and N−H sites (Figure 15) to be 47 cm^{-1} upshifted due to PB−PB HB (sites E, F), with an additional 5 cm^{-1} upshift due to PB−*water* HB (sites D and D*).[89] Thus, the $AmIII_3$ frequency of a long α-helix in water is expected to show an $AmIII_3$ band 52 cm^{-1} upshifted when compared to the fictitious case of an identical three-dimensional structure where no HB occurred.

Ham et al.[81] α-helix hydration studies suggest that for a polyalanine α-helix, only one water molecule (on average) HBs, and that this water HBs to the carbonyl oxygen. The water HB results in only an additional ~5 cm^{-1} upshift, as observed by Pimenov et al.,[89] because the water HB to the adjacent $(i + 4)$ PB carbonyl weakens the $(i + 4)$C═O···H−N(i) HB as explained by Schmidt et al.[77]

It should be noted that α-helices consisting of amino acid residues with larger side chains than ala will be less hydrated than are polyalanine α-helices,[112] and their $AmIII_3$ frequency should be less upshifted. Thus, α-helical segments of real proteins will be, in general, less upshifted because they will be involved in less PB−*water* HB.

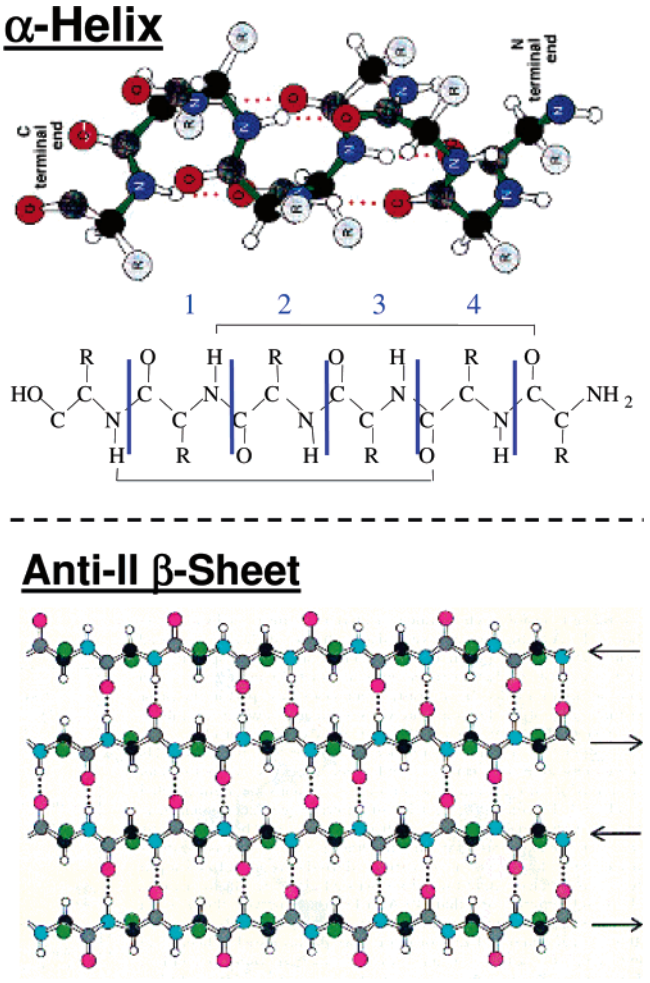

Figure 14. Diagram of α-helix and antiparallel (anti-II) β-sheet PB−PB HB patterns. Note: Both α-helical segment of $N \geq 7$ residues long and β-sheet segment of $n \geq 3$ strands contain three types of PBs, which differ in PB−PB HB (see text and Figures 15−17 for detail).

We can easily estimate the $AmIII_3$ frequency upshift for the three PB N-terminal residues that are PB−PB HB at their C═O sites from Schmidt et al.'s[77] AmII upshifts due to PB−PB HB (Figure 16). We expect the $AmIII_3$ frequency to be 12 cm^{-1} upshifted due to PB−PB HB (site F), with an additional 11 cm^{-1} upshift due to PB−*individual water* HB (site D)[77] or 16 cm^{-1} due to PB−*water sheath* HB (site D, Figure 16). An additional 33 cm^{-1} upshift comes from HB of their N−H group to water clusters at sites B (eq 13). Thus, we calculate a total $AmIII_3$ frequency upshift of 61 cm^{-1}.

In contrast, the PBs of the three C-terminal residues (Figure 17) will show a 35 cm^{-1} upshift due to PB−PB HB at the N−H site (E), with an additional 31 cm^{-1} upshift due to HB of the C═O to two waters at sites A and C, as can be estimated from eq 13 (total 66 cm^{-1}). However, the additional PB−*water* HB at site D* of the neighboring PB (Figures 12 and 17) will cause an 11 cm^{-1} $AmIII_3$ frequency downshift. Thus, the total $AmIII_3$ frequency upshift for the three C terminal PBs of an α-helix will be 55 cm^{-1}.

These considerations indicate that there is no more than a 9 cm^{-1} $AmIII_3$ frequency difference (Figures 6 and 15−17) between any of the different α-helical HB states in water, given that the PB is constrained to be at the α-helix Ψ angle. In contrast, the terminal six α-helical residues of anhydrous α-helices which are not bound to water could show $AmIII_3$ frequencies 35 and/or 12 cm^{-1} below that of the interior of the α-helix (Figures 7 and 15−17).

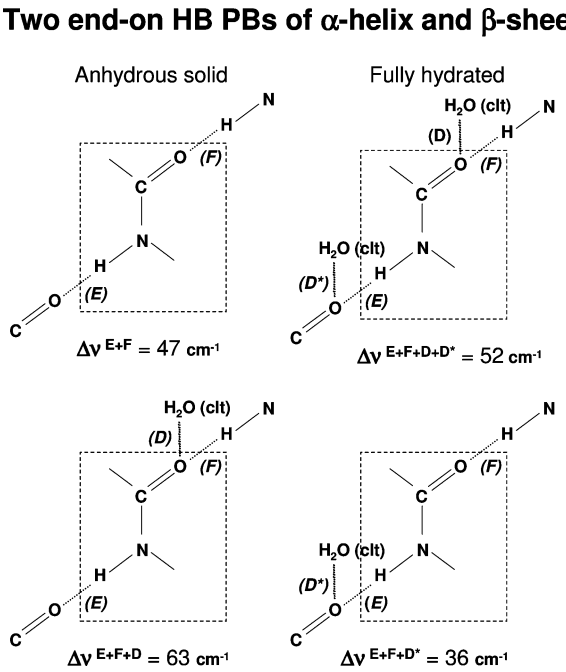

Figure 15. $AmIII_3$ frequency upshifts due to two-end-on HB; i.e., for interior PBs of α-helix and for PBs of interior strands of β-sheet. Note: 46 cm^{-1} $AmIII_3$ upshifts are estimated from the neat NMA (Figure 7) and anhydrous α-helix data, while 51 cm^{-1} upshifts are measured from α-helix in water data of Pimenov et al.[89] The individual upshifts upon HB at sites D and D* are estimated from the calculated AmII frequencies of NMA.[77]

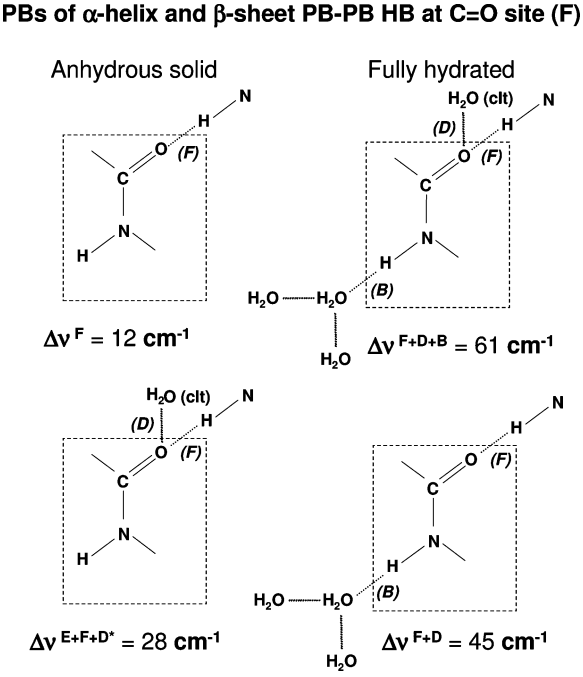

Figure 16. HB pattern and $AmIII_3$ frequency upshifts due to HB of PBs, which are PB−PB HB at their C═O sites; i.e., for the three N-terminal PBs of α-helices and half of PBs of exterior strands of β-sheet. Note: all these $AmIII_3$ upshifts were estimated from the calculated AmII frequencies of NMA.[77]

The impact of this $AmIII_3$ HB dependence on the measured UVRR spectra of our α-helical 21-residue AP peptide depends on the detailed melting behavior. If melting conformations followed the all-or-none α-helix peptide model,[22] the UVRR spectra of α-helical AP would be dominated by the interior α-helix PBs whose $AmIII_3$ frequencies are upshifted by 52 cm^{-1} due to PB−PB and water HB. The three C-terminal residues

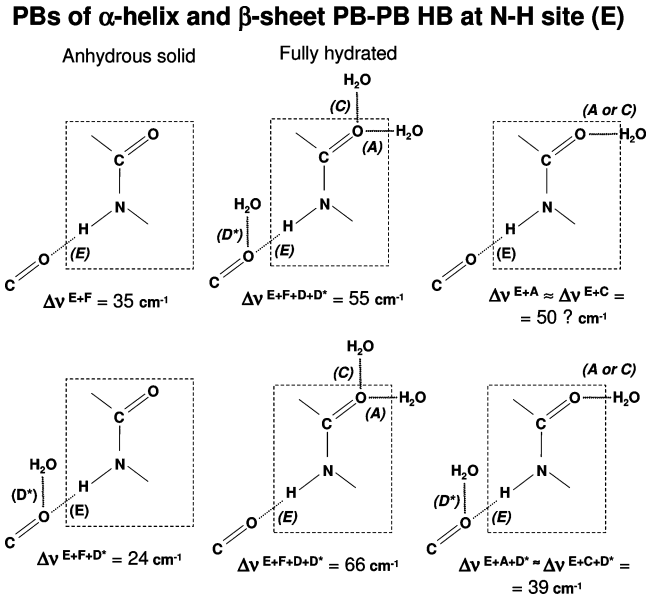

Figure 17. HB pattern and AmIII$_3$ frequency upshifts due to HB of PBs, which are PB−PB HB at their N−H site. These include the three C-terminal PBs of α-helix and half of PBs of exterior strands of β-sheet. Note: all these AmIII$_3$ upshifts were estimated from the calculated AmII upshifts of NMA.[77]

would be shifted by 61 cm^{-1}, while the three N-terminal residues would by shifted by 55 cm^{-1}. Thus, the AmIII$_3$ would be slightly broadened by the contributions of the terminal residues.

In contrast, the relative contributions of the interior α-helix PBs will decrease if we assume the zipper model where a distribution of α-helical lengths occur.[29] In fact it appears that an examination of the AmIII$_3$ band shape might allow us to distinguish the all-or-none versus the zipper model behaviors.

Thus, in the case AmIII$_3$ upshift of AP α-helix ($T_0 = 0$ °C), which is dominated by two-end-on PB−PB HB, we write

$$\Delta\nu^{\alpha-\mathrm{Helix}}(\mathrm{HB},T_0) \cong [n^{\mathrm{E}}\,\Delta\nu^{\mathrm{E}}_{\mathrm{P-P}} + n^{\mathrm{F}}\,\Delta\nu^{\mathrm{F}}_{\mathrm{P-P}}] + n^{\mathrm{D,D^*}}\,\Delta\nu^{\mathrm{D,D^*}}_{\mathrm{P-W}} \cong [n^{\mathrm{E}}\cdot 35\ \mathrm{cm}^{-1} + n^{\mathrm{F}}\cdot 12\ \mathrm{cm}^{-1}] + n^{\mathrm{D,D^*}}\cdot 5\ \mathrm{cm}^{-1} \quad (15)$$

Dependence of AmIII$_3$ Frequency on β-Sheet HB. Figure 14 shows a schematic diagram of an antiparallel β-sheet structure. The total number of PB−PB HBs formed in antiparallel and parallel β-sheet depends on the number of participating single peptide strands. In a double-stranded β-sheet, half of the water exposed PBs are involved in both PB−PB C═O HB (site F) and C═O PB−*water* HB (sites D and D*, Figure 16), while their N−H groups HB to *water* (site B, Figure 16), and the other half participate in N−H PB−PB HB (E site, Figure 17) while their C═O groups HB to water (sites A and C, Figure 17).

Interior strand PBs of multiple-strand β-sheets participate in two PB−PB HBs (sites E and F, Figure 15) and additionally may have C═O PB−water HB (sites D and D*, Figure 15). The PBs of their exterior strands will have the same HB pattern as those of double-stranded β-sheets (Figures 16 and 17).

Since each PB is expected to independently contribute to the AmIII region,[61,62] we expect that the β-sheet spectrum will contain overlapping contributions of the three different HB species which have the same β-strand-like Ramachandran angles, but different HB patterns (Figures 15−17; Table 1).

HB Shifts for β-Sheet Assuming α-Helix-Like PB−PB HB Strengths. If PB−PB HBs in antiparallel β-sheet are equivalent to those in α-helices (eq 15), we expect that half of the PBs (Figures 14 and 16) of exterior strands of β-sheet will show AmIII$_3$ bands, which are 12 cm^{-1} upshifted due to the C═O PB−PB HB (site F), 16 cm^{-1} upshifted due to the additional PB−*water clusters* HB (sites D), and 33 cm^{-1} upshifted due to N−H PB−water clusters HB at site B, for a total upshift of 61 cm^{-1} (Figure 16).

In contrast, the other half of PBs from exterior strands of a β-sheet (Figure 17) will produce an AmIII$_3$ band, which is 35 cm^{-1} upshifted due to N−H PB−PB HB (site E) and 31 cm^{-1} upshifted due to two C═O PB−*water* HB at sites A and C. However, the additional PB−*water sheath* HB at site D* of the neighboring PB reduces the AmIII$_3$ frequency by 11 cm^{-1}, giving a total AmIII$_3$ frequency upshift of 55 cm^{-1} (Figure 17).

In contrast, the interior PBs in β-sheet strands will have the HB pattern shown in Figure 15 and will show an AmIII$_3$ band which is 47 cm^{-1} upshifted due to both N−H and C═O PB−PB HBs (sites E and F) and 5 cm^{-1} upshifted due to an additional C═O PB−*water* HB at sites D and D*, for a total upshift of 52 cm^{-1} (Table 2). Thus, the maximum AmIII$_3$ frequency difference which can result due to different β-sheet hydration states, given identical β-sheet Ψ angles, is only 9 cm^{-1}.

The PLL−PGA antiparallel β-sheet structure is multistranded. Thus, its UVRR spectra are dominated by its interior strand PBs (Figure 15). The antiparallel β-sheet chains have their PB more exposed to water than occurs in an α-helix. Although water could HB to the β-sheet carbonyls from both sides, it is unlikely that more than one water/water cluster will HB to each C═O (Figure 15). Thus, we estimate that PB−*water* HB at sites D and D* for a β-sheet will also cause a 5 cm^{-1} upshift of the AmIII$_3$ frequency of the PBs in the interior β-sheet strands. Because HB at sites D and D* compensate,[77] differing PB−water HB strengths in β-sheets from those in α-helices would cause only small differences in the AmIII$_3$ frequency upshifts (Figure 15).

We achieve a similar conclusion by using a second independent argument which allows the possibility that the β-sheet PB−PB HB strengths may be somewhat weaker than those in α-helices.[115] We can calculate the AmIII$_3$ band frequencies of two non-HB β-strand-like conformations with similar Ψ angles. We measured a 1247 cm^{-1} (at 0 °C) AmIII$_3$ frequency for the PPII conformation of XAO[42,43] and a 1227 cm^{-1} (at 0 °C) frequency for an antiparallel β-sheet of a PLL−PGA mixture.[60] PPII and antiparallel β-sheets have similar Ψ angles of 145° and 135°, respectively.

We can calculate the downshifts which would occur if their HB were removed, while maintaining their conformations. The PPII AmIII$_3$ frequency in water at 0 °C is expected to be 64 cm^{-1} upshifted with "anhydrous PPII" (Figure 10) which gives a 1183 cm^{-1} AmIII$_3$ frequency for this fictitious isolated PPII (Ψ∼145°, Table 1). From the correlation in eq 5 above we conclude that the AmIII$_3$ frequency of an isolated non-HB β-strand will be at 1174 cm^{-1}.

Antiparallel PLL−PGA β-sheets (Ψ ∼ 135°) participate in both PB−PB and PB−water HBs. We estimate 48 cm^{-1} of this upshift derives from the PB−PB HB.

$$\Delta\nu^{\beta-\ \mathrm{sheet}}_{\mathrm{P-P}} \approx 1227 - 1174 + 5 \approx 48\ \mathrm{cm}^{-1} \quad (16)$$

Thus, the upshift value of 48 cm^{-1} due to PB−PB HB in PLL−PGA antiparallel β-sheet, estimated by eq 16, is very close to the 46 cm^{-1} value for PB−PB HB in NMA (eq 14). We will utilize a refined value of 47 cm^{-1} and assign an AmIII$_3$ 1175

cm^{-1} frequency to an isolated non-HB β-strand ($\Psi \sim 135°$). Thus, for PLL−PGA β-sheet in water at 0 °C we write

$$\Delta\nu_{P-P}^{\beta-\text{sheet}} \cong [n^{E}\,\Delta\nu_{P-P}^{E} + n^{F}\,\Delta\nu_{P-P}^{F} + n^{D}\,\Delta\nu_{P-W}^{D} n^{D} + n^{D^*}\,\Delta\nu_{P-W}^{D^*} n^{D^*} \approx [n^{E}\cdot 35\ \text{cm}^{-1} + n_{P-P}^{F}\cdot 12\ \text{cm}^{-1} + n_{P-W}^{D,D^*}\cdot 5\ \text{cm}^{-1}] \quad (17)$$

where all the parameters have the same meaning as in eq 15.

Temperature Dependence of $AmIII_3$ Frequency. The $AmIII_3$ UVRR bands as well as AmI and AmII bands of the pure secondary structure conformations show monotonic frequency shifts with temperature that are independent of conformational changes.[22,29,42,43] These monotonic frequency shifts occur due to a decrease in the PB-to-water HB strength as the temperature increases.[42,43,80,81,105,112−114] For example, in the case of XAO peptide, which is in a highly hydrated PPII conformation, the $AmIII_3$ band monotonically downshifts with an increase of temperature with a slope of $-0.11\ \text{cm}^{-1}/°\text{C}$.[43]

Thus, we can write for PPII conformation

$$\Delta\nu_{III}^{PPII}(T) \cong (T - T_0)\left(\frac{\partial\nu^{A} + \partial\nu^{B} + \partial\nu^{C}}{\partial T}\right) = -0.11(T - T_0)\ \text{cm}^{-1} \quad (18)$$

where $T_0 = 0$ °C.

Assuming the similar HB pattern for 2.5_1-helix, we can write

$$\Delta\nu_{III}^{2.5_1-\text{Helix}}(T) \cong \Delta\nu_{III}^{PPII}(T) = -0.11(T - T_0)\ \text{cm}^{-1} \quad (19)$$

We can generalize this result for any extended β-strand structure, i.e., any extended structure consisting of a single strand with Ψ and Φ Ramachandran angles in the β-strand region of the Ramachandran plot

$$\Delta\nu_{III}^{EXTENDED}(T) \cong \Delta\nu_{III}^{PPII}(T) = -0.11(T - T_0)\ \text{cm}^{-1} \quad (20)$$

We recently measured the temperature slope of the frequency shifts of the $AmIII_3$ and other amide bands for systems dominated by PB−PB HB, for the pure β-sheet[60] and pure α-helix[42,89] conformations and for neat NMA (Figure 11, Table 4). The temperature slopes for neat NMA are ~40% less than that of fully hydrated NMA (Table 4). In contrast, in water we found much smaller $AmIII_3$ shifts for two-end-on HB (Figure 15) α-helix[42,89] and β-sheet[60] conformations at the edge of measurability

$$\Delta\nu_{III}^{\alpha-\text{Helix}}(T) \cong \Delta\nu_{III}^{\beta-\text{Sheet}}(T) \approx 0\ \text{cm}^{-1} \quad (21)$$

The smaller dependence of the amide band frequencies on temperature in the α-helix and β-sheet intramolecularly hydrogen bonded structures results from the collective nature of the extensive hydrogen bonding network, which requires more perturbation to significantly change the average hydrogen bond lengths.

Generalizing, we can write for monotonic frequency shifts of $AmIII_3$ band of any conformation

$$\Delta\nu_{III}(T) \cong \delta\{-0.11(T - T_0)\}\ \text{cm}^{-1} \quad (22)$$

where δ is a parameter, which mainly reflects the degree of hydration of a particular secondary structure element and which we set at this time equal to "0" for long α-helix and multistranded β-sheet, and is equal to "1" in the case of PPII, 2.5_1-helix, or any extended β-strand-like conformation consisting of a single strand.

We estimate δ to be 0.8 for both the three N-terminal PB in α-helices and the exterior PB in β-sheet strands (Figure 16). In contrast, we estimate δ to be ~0.5 for both the *three C-terminal PB of α-helices* and the exterior *PB of β-sheet strands* (Figure 17). These estimates derive from the assumption that the temperature dependence originates from PB−*water* HB strength changes and that the relative frequency dependence scales with the extent of water HB frequency upshift compared to that found in the PPII conformation.

Quantitative Correlation of the $AmIII_3$ Frequency to the PB Ψ Ramachandran Angle, and HB. Inserting eqs 5, 13, 15, 17, and 22 into the eq 9, we obtain the following general expression, which relates the $AmIII_3$ frequency, Ψ Ramachandran angle and HB

$$\nu_{III3}(\Psi,T,\text{HB}) = [1192\ \text{cm}^{-1} - 54\ \text{cm}^{-1}\sin(\Psi + 26°)] + [n_{P-P}^{E}\cdot 35\ \text{cm}^{-1} + n_{P-P}^{F}\cdot 12\ \text{cm}^{-1} + n_{P-W}^{D,D^*}\cdot 5\ \text{cm}^{-1}] + [n_{P-W}^{A}\cdot 15\ \text{cm}^{-1} + n_{P-W}^{B}\cdot 33\ \text{cm}^{-1} + n_{P-W}^{C}\cdot 16\ \text{cm}^{-1}] + \delta\left\{-0.11\,\frac{\text{cm}^{-1}}{°\text{C}}\,(T - T_0)\right\} \quad (23)$$

where all the parameters are described above.

For ease of use we have decomposed eq 23 into three different families of equations which are listed as eqs 5, 6A−D, and 7A−C. These are each specific to particular secondary structures with their particular HB patterns as described above in the Results and Discussion section of this paper. We also created an "average" eq 6E for estimation of Ψ Ramachandran angle of a PB in aqueous solution, if the HB state of a PB is unknown.

References and Notes

(1) Kuszewski, J.; Schwieters, C. D.; Garrett, D. S.; Byrd, R. A.; Tjandra, N.; Clore, G. M. *J. Am. Chem. Soc.* **2004**, *126*, 6258.

(2) Tugarinov, V.; Hwang, P. M.; Kay, L. E. *Annu. Rev. Biochem.* **2004**, *73*, 107.

(3) Dyson, H. J.; Wright, P. E. *Chem. Rev.* **2004**, *104*, 3607.

(4) Sattler, M.; Schleucher, J.; Griesinger, C. *Prog. Nucl. Magn. Reson. Spectrosc.* **1999**, *34*, 93.

(5) Wider, G.; Wuthrich, K. *Curr. Opin. Struct. Biol.* **1999**, *9*, 594.

(6) Clore, G. M.; Gronenborn, A. M. *Proc. Natl. Acad. Sci. U.S.A.* **1998**, *95*, 5891.

(7) Campbell-Burk, S.; Zhong, S. *Curr. Opin. Biotechnol.* **1994**, *5*, 346.

(8) Bax, A.; Grzesiek, S. *Acc. Chem. Res.* **1993**, *26*, 131.

(9) Billeter, M. *Q. Rev. Biophys.* **1992**, *25*, 325.

(10) Bonmatin, J. M.; Genest, M.; Petit, M. C.; Gincel, E.; Simorre, J. P.; Cornet, B.; Gallet, X.; Caille, A.; Labbe, H.; Vovelle, F.; Ptak, M. *Biochimie* **1992**, *74*, 825.

(11) Wagner, G.; Hyberts, S. G.; Havel, T. F. *Annu. Rev. Biophys. Biomol. Struct.* **1992**, *21*, 167.

(12) MacKenzie, N. E.; Gooley, P. R.; Hardaway, L. A. *Annu. Rev. Physiol.* **1992**, *54*, 749.

(13) James, T. L.; Basus, V. J. *Annu. Rev. Phys. Chem.* **1991**, *42*, 501.

(14) Hass, M. A. S.; Thuesen, M. H.; Christensen, H. E. M.; Led, J. J. *J. Am. Chem. Soc.* **2004**, *126*, 753.

(15) Palmer, A. G., III.; Grey, M. J.; Wang, C. *Methods Enzymol.* **2005**, *394*, 430.

(16) Asher, S. A. *Handbook of Vibrational Spectroscopy*; John Wiley & Sons: New York, 2001; Vol. 1, p 557.

(17) Schweitzer-Stenner, R. *J. Raman Spectrosc.* **2001**, *32*, 711.

(18) Thomas, G. J., Jr. *Annu. Rev. Biophys. Biomol. Struct.* **1999**, *28*, 1.

(19) Spiro, T. G.; Czernuszewicz, R. S. *Methods Enzymol.* **1995**, *246*, 416.

(20) Austin, J. C.; Jordan, T.; Spiro, T. G. *Adv. Spectrosc.* (*Chichester, U.K.*) **1993**, *20*, 55.

(21) Tuma, R.; Russell, M.; Rosendahl, M.; Thomas, G. J., Jr. *Biochemistry* **1995**, *34*, 15150.

(22) Lednev, I. K.; Karnoup, A. S.; Sparrow, M. C.; Asher, S. A. *J. Am. Chem. Soc.* **1999**, *121*, 8074.

(23) Huang, C.-Y.; Balakrishnan, G.; Spiro, T. G. *Abstracts of Papers*, 229th ACS National Meeting, San Diego, CA, United States, March 13−17, 2005; American Chemical Society: Washington, DC, 2005, INOR.
(24) Gulotta, M.; Rogatsky, E.; Callender, R. H.; Dyer, R. B. *Biophys. J.* **2003**, *84*, 1909.
(25) Rubtsov, I. V.; Wang, J.; Hochstrasser, R. M. *J. Phys. Chem. A* **2003**, *107*, 3384.
(26) Callender, R.; Dyer, R. B. *Curr. Opin. Struct. Biol.* **2002**, *12*, 628.
(27) Haruta, N.; Kitagawa, T. *Biochemistry* **2002**, *41*, 6595.
(28) Pan, D.; Ganim, Z.; Kim, J. E.; Verhoeven, M. A.; Lugtenburg, J.; Mathies, R. A. *J. Am. Chem. Soc.* **2002**, *124*, 4857.
(29) Lednev, I. K.; Karnoup, A. S.; Sparrow, M. C.; Asher, S. A. *J. Am. Chem. Soc.* **2001**, *123*, 2388.
(30) Wang, J.; El-Sayed, M. A. *Biophys. J.* **2001**, *80*, 961.
(31) Yamamoto, K.; Mizutani, Y.; Kitagawa, T. *Biophys. J.* **2000**, *79*, 485.
(32) Hamm, P.; Lim, M.; Hochstrasser, R. M. *J. Phys. Chem. B* **1998**, *102*, 6123.
(33) Hochstrasser, R. M. *Ultrafast Processes Chem. Photobiol.* **1995**, 163.
(34) Spiro, T. G.; Smulevich, G.; Su, C. *Biochemistry* **1990**, *29*, 4497.
(35) Tuma, R. *J. Raman Spectrosc.* **2005**, *36*, 307.
(36) Jarzecki, A. A.; Spiro, T. G. *J. Phys. Chem. A* **2005**, *109*, 421.
(37) Venkateshrao, S.; Yin, J.; Jarzecki, A. A.; Schultz, P. G.; Spiro, T. G. *J. Am. Chem. Soc.* **2004**, *126*, 16361.
(38) Chi, Z.; Chen, X. G.; Holtz, J. S. W.; Asher, S. A. *Biochemistry* **1998**, *37*, 2854.
(39) Copeland, R. A.; Spiro, T. G. *Biochemistry* **1987**, *26*, 2134.
(40) Lord, R. C. *Appl. Spectrosc.* **1977**, *31*, 187.
(41) Overman, S. A.; Bondre, P.; Maiti, N. C.; Thomas, G. J., Jr. *Biochemistry* **2005**, *44*, 3091.
(42) Mikhonin, A. V.; Ahmed, Z.; Ianoul, A.; Asher., S. A. *J. Phys. Chem. B* **2004**, *108*, 19020.
(43) Asher, S. A.; Mikhonin, A. V.; Bykov, S. B. *J. Am. Chem. Soc.* **2004**, *126*, 8433.
(44) Cai, S.; Singh, B. R. *Biochemistry* **2004**, *43*, 2541.
(45) Ozaki, Y.; Murayama, K.; Wu, Y.; Czarnik-Matusewicz, B. *Spectroscopy* (*Amsterdam, Neth.*) **2003**, *17*, 79.
(46) Blanch, E. W.; Hecht, L.; Barron, L. D. *Methods* (*San Diego, CA, U.S.*) **2003**, *29*, 196.
(47) Asher, S. A.; Ianoul, A.; Mix, G.; Boyden, M. N.; Karnoup, A.; Diem, M.; Schweitzer-Stenner, R. *J. Am. Chem. Soc.* **2001**, *123*, 11775.
(48) Jung, Y. M.; Czarnik-Matusewicz, B.; Ozaki, Y. *J. Phys. Chem. B* **2000**, *104*, 7812.
(49) Vedantham, G.; Sparks, H. G.; Sane, S. U.; Tzannis, S.; Przybycien, T. M. *Anal. Biochem.* **2000**, *285*, 33.
(50) Vecchio, G.; Zambianchi, F.; Zacchetti, P.; Secundo, F.; Carrea, G. *Biotechnol. Bioeng.* **1999**, *64*, 545.
(51) Baello, B. I.; Pancoska, P.; Keiderling, T. A. *Anal. Biochem.* **1997**, *250*, 212.
(52) Bramanti, E.; Benedetti, E.; Sagripanti, A.; Papineschi, F.; Benedetti, E. *Biopolymers* **1997**, *41*, 545.
(53) Colaianni, S. E. M.; Aubard, J.; Hansen, S. H.; Nielsen, O. F. *Vib. Spectrosc.* **1995**, *9*, 111.
(54) Griebenow, K.; Klibanov, A. M. *Proc. Natl. Acad. Sci. U.S.A.* **1995**, *92*, 10969.
(55) Jordan, T.; Spiro, T. G. *J. Raman Spectrosc.* **1994**, *25*, 537.
(56) Fu, F.-N.; DeOliveira, D. B.; Trumble, W. R.; Sarkar, H. K.; Singh, B. R. *Appl. Spectrosc.* **1994**, *48*, 1432.
(57) DeGrazia, H.; Harman, J. G.; Tan, G. S.; Wartell, R. M. *Biochemistry* **1990**, *29*, 3557.
(58) Roberts, G. M.; Lee, O.; Calienni, J.; Diem, M. *J. Am. Chem. Soc.* **1988**, *110*, 1749.
(59) Ianoul, A.; Boyden, M. N.; Asher, S. A. *J. Am. Chem. Soc.* **2001**, *123*, 7433.
(60) Mikhonin, A. V.; Myshakina, N. S.; Bykov, S. V.; Asher, S. A. *J. Am. Chem. Soc.* **2005**, *127*, 7712.
(61) Mikhonin, A. V.; Asher, S. A. *J. Phys. Chem. B* **2005**, *109*, 3047.
(62) Mix, G.; Schweitzer-Stenner, R.; Asher, S. A. *J. Am. Chem. Soc.* **2000**, *122*, 9028.
(63) Fang, C.; Wang, J.; Charnley, A. K.; Barber-Armstrong, W.; Smith, A. B.; Decatur, S. M.; Hochstrasser, R. M. *Chem. Phys. Lett.* **2003**, *382*, 586.
(64) Dudik, J. M.; Johnson, C. R.; Asher, S. A. *J. Phys. Chem.* **1985**, *89*, 3805.
(65) Robin, M. B. *Higher Excited States of Polyatomic Molecules*; Academic Press: New York, 1975; Vol. II.
(66) Chen, X. G.; Asher, S. A.; Schweitzer-Stenner, R.; Mirkin, N. G.; Krimm, S. *J. Am. Chem. Soc.* **1995**, *117*, 2884.
(67) Ianoul, A.; Mikhonin, A.; Lednev, I. K.; Asher, S. A. *J. Phys. Chem. A* **2002**, *106*, 3621.
(68) Chen, X. G.; Schweitzer-Stenner, R.; Asher, S. A.; Mirkin, N. G.; Krimm, S. *J. Phys. Chem.* **1995**, *99*, 3074.
(69) Garcia, A. E.; Onuchic, J. N. *Structure* (*Cambridge, MA, U.S.*) **2005**, *13*, 497.
(70) Snow, C. D.; Sorin, E. J.; Rhee, Y. M.; Pande, V. S. *Annu. Rev. Biophys. Biomol. Struct.* **2005**, *34*, 43.
(71) Rhee, Y. M.; Sorin, E. J.; Jayachandran, G.; Lindahl, E.; Pande, V. S. *Proc. Natl. Acad. Sci. U.S.A.* **2004**, *101*, 6456.
(72) Bykov, S. V.; Lednev, I. K.; Ianoul, A.; Mikhonin, A. V.; Asher, S. A. *Appl. Spectrosc.*, **2005**, *59*, 1541.
(73) Mirkin, N. G.; Krimm, S. *J. Phys. Chem. A* **2002**, *106*, 3391.
(74) Kubelka, J.; Keiderling, T. A. *J. Phys. Chem. A* **2001**, *105*, 10922.
(75) Besley, N. A. *J. Phys. Chem. A* **2004**, *108*, 10794.
(76) Torii, H.; Tatsumi, T.; Tasumi, M. *J. Raman Spectrosc.* **1998**, *29*, 537.
(77) Schmidt, P.; Dybal, J.; Rodriguez-Cabello, J. C.; Reboto, V. *Biomacromolecules* **2005**, *6*, 697.
(78) Torii, H.; Tatsumi, T.; Kanazawa, T.; Tasumi, M. *J. Phys. Chem. B* **1998**, *102*, 309.
(79) Torii, H.; Tatsumi, T.; Tasumi, M. *Mikrochim. Acta, Suppl.* **1997**, *14*, 531.
(80) Gnanakaran, S.; Hochstrasser, R. M.; Garcia, A. E. *Proc. Natl. Acad. Sci. U.S.A.* **2004**, *101*, 9229.
(81) Ham, S.; Hahn, S.; Lee, C.; Kim, T.-K.; Kwak, K.; Cho, M. *J. Phys. Chem. B* **2004**, *108*, 9333.
(82) Del Bene, J. E.; Jordan, M. J. T. *Int. Rev. Phys. Chem.* **1999**, *18*, 119.
(83) Bakker, H. J.; Nienhuys, H. K. *Science* **2002**, *297*, 587.
(84) Chaban, G. M.; Gerber, R. B. *J. Chem. Phys.* **2001**, *115*, 1340.
(85) Henri-Rousseau, O.; Blaise, P. *Chem. Phys.* **1999**, *250*, 249.
(86) Torii, H. *J. Phys. Chem. A* **2004**, *108*, 7272.
(87) Cheatum, C. M.; Tokmakoff, A.; Knoester, J. *J. Chem. Phys.* **2004**, *120*, 8201.
(88) Schweitzer-Stenner, R.; Eker, F.; Huang, Q.; Griebenow, K.; Mroz, P. A.; Kozlowski, P. M. *J. Phys. Chem. B* **2002**, *106*, 4294.
(89) Pimenov, K. V.; Bykov, S. V.; Mikhonin, A. V.; Asher, S. A. *J. Am. Chem. Soc.* **2005**, *127*, 2840.
(90) Lovell, S. C.; Davis, I. W.; Arendall, W. B., III.; de Bakker, P. I. W.; Word, J. M.; Prisant, M. G.; Richardson, J. S.; Richardson, D. C. *Proteins* **2003**, *50*, 437.
(91) Ho, B. K.; Thomas, A.; Brasseur, R. *Protein Sci.* **2003**, *12*, 2508.
(92) Kleywegt, G. J.; Jones, T. A. *Structure* (*London, U.K.*) **1996**, *4*, 1395.
(93) Yennawar, H. P.; Natarajan, S.; Viswamitra, M. A. *Int. J. Peptide Protein Res.* **1991**, *38*, 569.
(94) Fletterick, R. J.; Tsai, C. C.; Hughes, R. E. *J. Phys. Chem.* **1971**, *75*, 918.
(95) Eggleston, D. S.; Hodgson, D. J. *Int. J. Peptide Protein Res.* **1983**, *21*, 288.
(96) Gorbitz, C. H. *Acta Crystallogr.* **2000**, *C56*, 500.
(97) Eggleston, D. S. *Acta Crystallogr.* **1984**, *C40*, 1250.
(98) Jones, P. G.; Falvello, L.; Kennard, O. *Acta Crystallogr.* **1978**, *B34*, 1939.
(99) Chaturvedi, S.; Go, K.; Parthasarathy, R. *Biopolymers* **1991**, *31*, 397.
(100) Lednev, I. K.; Ermolenkov, V. V.; He, W.; Xu, M. *Anal. Bioanal. Chem.* **2005**, *381*, 431.
(101) Dixon, D. A.; Dobbs, K. D.; Valentini, J. J. *J. Phys. Chem.* **1994**, *98*, 13435.
(102) Guo, H.; Karplus, M. *J. Phys. Chem.* **1992**, *96*, 7273.
(103) Jorgensen, W. L.; Swenson, C. J. *J. Am. Chem. Soc.* **1985**, *107*, 1489.
(104) Huang, H.; Malkov, S.; Coleman, M.; Painter, P. *J. Phys. Chem. A* **2003**, *107*, 7697.
(105) Avbelj, F.; Luo, P.; Baldwin, R. L. *Proc. Natl. Acad. Sci. U.S.A.* **2000**, *97*, 10786.
(106) Herrebout, W. A.; Clou, K.; Desseyn, H. O. *J. Phys. Chem. A* **2001**, *105*, 4865.
(107) Noda, I.; Liu, Y.; Ozaki, Y. *J. Phys. Chem.* **1996**, *100*, 8665.
(108) Fleming, P. J.; Fitzkee, N. C.; Mezei, M.; Srinivasan, R.; Rose, G. D. *Protein Sci.* **2005**, *14*, 111.
(109) Bochicchio, B.; Tamburro, A. M. *Chirality* **2002**, *14*, 782.
(110) Shi, Z.; Woody, R. W.; Kallenbach, N. R. *Adv. Protein Chem.* **2002**, *62*, 163.
(111) Mayne, L. C.; Hudson, B. *J. Phys. Chem.* **1991**, *95*, 2962.
(112) Walsh, S. T. R.; Cheng, R. P.; Wright, W. W.; Alonso, D. O. V.; Daggett, V.; Vanderkooi, J. M.; DeGrado, W. F. *Protein Sci.* **2003**, *12*, 520.
(113) Manas, E. S.; Getahun, Z.; Wright, W. W.; DeGrado, W. F.; Vanderkooi, J. M. *J. Am. Chem. Soc.* **2000**, *122*, 9883.
(114) McColl, I. H.; Blanch, E. W.; Hecht, L.; Barron, L. D. *J. Am. Chem. Soc.* **2004**, *126*, 8181.
(115) Sheu, S.-y.; Yang, D.-y.; Selzle, H. L.; Schlag, E. W. *Proc. Natl. Acad. Sci. U.S.A.* **2003**, *100*, 12683.